

# Global Biogeochemical Cycles

## RESEARCH ARTICLE

10.1029/2020GB006665

### Key Points:

- Iron distributions in Antarctic sea ice largely differ among three formulations of iron incorporation, but fertilization effects are similar
- Sediments and iron transport by sea ice could work in synergy to fertilize areas remote from the coasts
- Iron incorporated into sea ice enhances Southern Ocean primary production by 5–10% and carbon export by 9–19%, depending on the formulation

### Supporting Information:

- Supporting Information S1

### Correspondence to:

R. Person,  
renaud.person@ird.fr

### Citation:

Person, R., Vancoppenolle, M., & Aumont, O. (2020). Iron incorporation from seawater into Antarctic sea ice: A model study. *Global Biogeochemical Cycles*, 34, e2020GB006665. <https://doi.org/10.1029/2020GB006665>

Received 14 MAY 2020

Accepted 19 OCT 2020

Accepted article online 31 OCT 2020

©2020. The Authors.

This is an open access article under the terms of the Creative Commons Attribution-NonCommercial License, which permits use, distribution and reproduction in any medium, provided the original work is properly cited and is not used for commercial purposes.

## Iron Incorporation From Seawater Into Antarctic Sea Ice: A Model Study

R. Person<sup>1,2</sup> , M. Vancoppenolle<sup>2</sup> , and O. Aumont<sup>2</sup> 

<sup>1</sup>Sorbonne Université, CNRS, IRD, MNHN, INRAE, ENS, UMS 3455, OSU Ecce Terra, Paris, France, <sup>2</sup>Sorbonne Université, CNRS, IRD, MNHN, UMR7159 LOCEAN-IPSL, Paris, France

Sea ice acts as an iron (Fe) reservoir in the Southern Ocean (SO) where primary productivity is largely Fe limited. The mechanisms leading to Fe enrichment in sea ice result from the combination of poorly understood and largely unexplored physical and biological processes. We analyze the biogeochemical impacts of three plausible idealized formulations of dissolved Fe (DFe) incorporation into sea ice corresponding to (i) constant Fe concentration in sea ice, (ii) constant ocean-ice Fe flux, and (iii) ocean-ice Fe flux linearly varying with seawater Fe concentration in a global ocean-sea-ice-biogeochemical model, focusing on the SO. The three formulations simulate different geographical distributions of DFe concentrations in sea ice. Iron in sea ice remains largely uncertain due to the limited number of spatial and seasonal observations, poorly constrained Fe sources and sinks, and significant uncertainties in simulated sea ice and hydrography. Despite these differences, the fertilization effect by sea ice on phytoplankton photosynthesis is qualitatively similar regardless of the formulation considered. Iron incorporation during sea-ice formation, transport, and melt release, common to all formulations, dominates over differences in sea-ice Fe concentrations. Formulating the Fe incorporation rate as proportional to seawater Fe concentrations gives the closest agreement to field observations. With this formulation, sediments work in synergy with Fe transport to fertilize the waters north of the continental shelf. Southern Ocean primary production and export production increase by 5–10% and 9–19%, respectively, when Fe incorporation into sea ice is considered, suggesting a moderate effect of Fe-bearing sea ice on marine productivity.

## 1. Introduction

Primary productivity in the Southern Ocean (SO) is largely limited by the availability of the micronutrient iron (Fe) (Boyd et al., 2007; Coale et al., 2004; de Baar et al., 1995, 1999; Martin et al., 1990; Smetacek, 2001). Together with light and temperature, Fe limitation shapes the spatial and temporal distribution of phytoplankton in the SO (Ardyna et al., 2017, 2019; Boyd, 2002; Boyd et al., 2012; Tagliabue et al., 2017) and modulates the magnitude of the biological carbon pump (Blain et al., 2007; Bowie et al., 2001; Boyd et al., 2007). However, several sources supply Fe to SO waters (Boyd & Ellwood, 2010): sediments estimated as the main source (Borrione et al., 2014; Tagliabue et al., 2009), hydrothermal activity (Ardyna et al., 2019), icebergs (Duprat et al., 2016; Lin et al., 2011), ice shelves (Dinniman et al., 2020; Gerringa et al., 2012; Herraiz-Borreguero et al., 2016), sea ice (Lannuzel et al., 2016), and atmospheric dust deposition as a nondominant source (Wagener et al., 2008).

A large part of the SO is under the influence of the cryosphere, which involves several forms of ice: sea ice (pack ice and landfast ice), icebergs, and melting ice shelves. These cryospheric elements reduce light availability at the ocean surface. However, they are also iron laden, which is thought to stimulate productivity and carbon export (Duprat et al., 2016; Lin et al., 2011; Raiswell et al., 2016; Wadley et al., 2014; Wang et al., 2014), to an extent that remains subject to large uncertainties (Hopwood et al., 2019; Person et al., 2019). Among these ice forms, sea ice is considered as one of the important Fe sources in the SO (Boyd & Ellwood, 2010; Geibert et al., 2010; Lannuzel et al., 2016; Tagliabue et al., 2017; Vancoppenolle et al., 2013), acting as a spatially extended reservoir, and transporting Fe from coastal to offshore regions, with coastal sediments being the main Fe source (Lancelot et al., 2009; Lannuzel et al., 2010; Sedwick & DiTullio, 1997; Wadley et al., 2014). The so-called sea-ice fertilization effect, induced by the release of Fe into surface waters in spring and summer, stimulates phytoplankton photosynthesis and primary productivity in the Antarctic marginal ice zone and polynyas (Arrigo et al., 1997; Lannuzel et al., 2010; Moreau et al., 2019; Sedwick & DiTullio, 1997).

The fact that Antarctic sea ice is considered as an important Fe source for SO waters is justified by Fe concentrations in sea ice at least 1 order of magnitude larger than in seawater (de Jong et al., 2013, 2015; Lannuzel et al., 2007, 2008, 2011, 2016; van der Merwe et al., 2011). This enrichment is in sharp contrast with salts and macronutrients which are generally much less abundant in sea ice than in seawater (Fripiat et al., 2017). Lannuzel et al. (2016) compiled all available Antarctic sea-ice Fe observations. Fifty-six ice cores and nearly 300 core sections are available, indicating a mean dissolved Fe (DFe) concentration of  $9.8 \pm 15 \text{ nmol L}^{-1}$ . By comparison, the mean seawater DFe concentration between 0 and 100 m depth, south of the Polar Front in the Antarctic zone, is  $0.38 \pm 0.55 \text{ nmol L}^{-1}$  (Tagliabue et al., 2012). Dissolved Fe concentrations in sea ice somehow increases with ice thickness, whereas sea-ice salinity and macronutrients decrease with thickness (Fripiat et al., 2017; Kovacs, 1996). In landfast sea ice (the ice attached to the coast), DFe is about twice as large as in pack ice (drifting sea ice). Particulate Fe (PFe) concentrations are generally much larger than DFe, regardless of the location. Observed PFe concentrations increase as the bathymetry decreases, suggesting a dominance of sedimentary Fe supply at stations collected nearest to the Antarctic continent. An overwhelming limitation of our knowledge is the paucity of observational data: Their spatial coverage is of only a few square meters, which is  $0.000\times\%$  of the maximum sea-ice extent (20 million  $\text{km}^2$ , as per Parkinson, 2019).

Iron incorporation into sea ice results from a series of physical and biological mechanisms, which remain highly hypothetical (see reviews by Janssens et al., 2016, & Lannuzel et al., 2016). Sediment particles and associated Fe can be incorporated in the water column, through ice nucleation or scavenging by rising frazil crystals, before they reach the sea-ice base, as highlighted in the Arctic (Dethleff, 2005). These water column processes, coupling ice nucleation and suspended particles, best explain the rapid DFe increase observed right after ice formation (Janssens et al., 2016), as well as the presence of Fe in granular ice (ice with randomly oriented crystals and originating from frazil ice) (Lannuzel et al., 2007). Iron incorporation into sea ice could also be favored by hydrodynamic processes, such as Langmuir circulation (Martin & Kauffman, 1981), wave pumping (Garrison et al., 1989), spring tides (de Jong et al., 2013), and brine convection within the bottom ice layers (Vancoppenolle et al., 2010). Iron-rich waters favor Fe incorporation, in particular near sediment sources, as suggested by summer land-fast sea ice cores from the McMurdo area (de Jong et al., 2013). Dissolved Fe within brine samples is generally much lower than retrieved from melted ice core sections, which suggests the adsorption of DFe onto something within sea ice (Lannuzel et al., 2016), possibly aided by the presence of Fe-binding organic ligands such as exopolysaccharides (Janssens et al., 2018; Lannuzel et al., 2007, 2015). This supposition is reinforced by the strong association of DFe with organic matter in sea ice, which suggests a prominent role of biology—for instance biological assimilation into growing algae or recycling by organic matter.

All these elements stress the need to consider the sea-ice Fe source in biogeochemical studies of the SO. However, in a context of rare observations and weak understanding of the processes at play, ocean modeling systems currently use very simple parameterizations for DFe incorporation into sea ice (Lancelot et al., 2009; Wadley et al., 2014; Wang et al., 2014). The different parameterizations produce large differences in the concentrations of DFe in Antarctic sea ice, both in terms of mean value and spatial distribution (Lancelot et al., 2009; Wang et al., 2014). Lancelot et al. (2009) assume a constant DFe concentration ( $16 \text{ nmol L}^{-1}$ ) in forming sea ice, provided there are sufficient stocks from underlying sea waters, leading to fairly homogeneous DFe sea-ice concentrations apart from two large regions of near-zero concentrations: One east from the Ross Sea to the Antarctic Peninsula and the second east of the Weddell Sea. Wang et al. (2014) assume that DFe concentration in growing ice is a fraction of seawater concentration, which is assumed to be higher when sediment particles are more abundant. Their approach results in relatively low DFe concentrations in sea ice ( $0.05\text{--}1.5 \text{ nmol L}^{-1}$ ), except in a small region west of the Antarctic Peninsula ( $\gg 20 \text{ nmol L}^{-1}$ ). The fertilization effect of the sea-ice Fe content released upon melting is estimated at 11% of SO total primary production in Wadley et al. (2014) and at less than 4% of export production in the region south of  $60^\circ\text{S}$  in Wang et al. (2014).

The large uncertainties surrounding the role played by sea ice on the Fe cycle, primary production, and carbon export and the lack of consensus between climate models on the sensitivity of sea ice to climate change in the SO (Maksym, 2019; Pörtner et al., 2019; Rintoul et al., 2018) highlight the need to explore the gray areas surrounding the role of sea ice as an Fe source. Here we investigate some of these

uncertainties by comparing the effects of three different idealized formulations of Fe uptake in growing sea ice within a global ocean-sea-ice-biogeochemical model. We specifically evaluate their effects on DFe concentrations in sea ice and surface seawater, on surface seawater chlorophyll concentrations, and on primary productivity and carbon export.

## 2. Method

### 2.1. Model Description

We use the ocean modeling system NEMO (Nucleus for European Modeling of the Ocean) Version 3.6 (Madec, 2008), which includes representations of ocean hydrodynamics, sea ice, and biogeochemistry. The model couples the ocean dynamical core OPA (Océan PARallélisé; Madec, 2008), the marine biogeochemistry model PISCES-v2 (Aumont et al., 2015), and the Louvain-la-Neuve sea Ice Model LIM3.6 (Rousset et al., 2015). We use NEMO in a global configuration at 2° horizontal resolution on a quasi-isotropic tripolar grid. The vertical grid follows a partial step  $z$ -coordinate scheme and has 31 levels, of which 20 are located in the first 500 m. Lateral mixing is computed along isoneutral surfaces (Madec, 2008). Mesoscale eddy-induced turbulence follows the Gent and McWilliams (1990) parameterization, and vertical mixing is parameterized using a turbulent kinetic energy scheme (Blanke & Delecluse, 1993) as modified by Madec (2008).

The biogeochemical model PISCES simulates two phytoplankton types (diatoms and nanophytoplankton), two zooplankton size classes (microzooplankton and mesozooplankton), the biogeochemical cycles of five limiting nutrients (nitrate, ammonium, phosphate, silicate, and iron), dissolved oxygen, dissolved inorganic carbon, total alkalinity, dissolved organic matter, and small and large organic particles. Different external sources of Fe are represented: atmospheric dust deposition, sediment mobilization, and river input. The Fe exchange with sea ice is implemented by a simple and non-conservative parameterization of the exchange of Fe between sea ice and seawater, sea ice acting as an external reservoir of Fe. A constant Fe concentration in this sea-ice reservoir is prescribed. In our study, this original parameterization is disabled. A complete description of the biogeochemical model PISCES can be found in Aumont et al. (2015).

The sea-ice model LIM 3.6 (Rousset et al., 2015) uses the classical Arctic Ice Dynamics Joint Experiment (AIDJEX) approach (Coon et al., 1974), treating thermodynamics as purely vertical and ice dynamics as purely horizontal. To resolve ice drift due to winds and currents, a 2-D plastic continuum is assumed, using the modified elastic-viscous-plastic method of Bouillon et al. (2013). Several ice growth and melt processes are considered: new ice formation in open water, basal growth and melt, snow-ice formation and seawater freezing into ridges, and surface melting. Dynamic variations in brine inclusions are considered using a prognostic sea-ice salinity, which changes due to brine drainage and sea-ice growth and melt (Vancoppenolle et al., 2009). Sea-ice state variables (ice volume, concentration, salt content, internal energy, snow volume, and snow internal energy) are transported with ice motion using the second-order momentum conserving scheme of Prather (1986). Subgrid-scale variations in ice properties are considered by using five ice thickness categories. Thermodynamics and dynamics (ridging and rafting) redistribute ice across different ice thickness categories (Lipscomb, 2001; Thorndike et al., 1975; Vancoppenolle et al., 2009).

### 2.2. Description of the Parameterizations of Dissolved Iron Incorporation Into Sea Ice

In the model configuration used in this study, DFe is a state variable, not only in the ocean as in the reference version but also in sea ice. The corresponding prognostic variable is the DFe content in sea ice expressed in  $\text{mmol m}^{-2}$ , computed for each sea-ice thickness category. The sea-ice DFe concentration can be diagnosed by dividing the content by the sea-ice volume per unit area (grid-cell mean thickness). Dissolved Fe in sea ice is considered as a passive tracer, that is, no chemical reactions, biological processes (Fe uptake or remineralization), and Fe speciation (ice processing redox, dissolution and precipitation reactions) are represented, even though Fe in glacial systems is estimated to be highly reactive (Raiswell et al., 2018). Dissolved Fe sea-ice content ( $\text{DFe}_i$ ) follows a conservation equation, similar to that of all other sea-ice state variables:

**Table 1**  
*Description of the Model Experiments*

Experiments	Ocean-to-sea-ice DFe flux during ice growth	Control parameter	Sediment source
CTL	$F_{Fe} = 0$		yes
CTLnoSED	$F_{Fe} = 0$		no
CST	$F_{Fe} = DFe_i \cdot \sum_{i=0}^n \Delta v_i / \Delta t$	$DFe_i = 10 \text{ nmol L}^{-1}$	yes
FLXCST	$F_{Fe} = F$	$F = 1.3 \cdot 10^{-6} \text{ nmol m}^{-2} \text{ s}^{-1}$	yes
FLXVAR	$F_{Fe} = k \cdot DFe_w$	$k = 4 \cdot 10^{-6} \text{ m s}^{-1}$	yes
FLXVAR2	$F_{Fe} = k \cdot DFe_w$	$k = 8 \cdot 10^{-6} \text{ m s}^{-1}$	yes
FLXVARnoSED	$F_{Fe} = k \cdot DFe_w$	$k = 4 \cdot 10^{-6} \text{ m s}^{-1}$	no

*Note.* In all cases, Fe uptake in sea ice is only active when the ice is growing. By contrast, when the ice is melting, an amount of Fe proportional to volume loss is released to the ocean.  $\Delta v$  = increase in ice volume per grid cell area;  $\Delta t$  = time step.

$$\frac{\partial DFe_i}{\partial t} = -\nabla \cdot (u DFe_i) + \theta + \psi. \quad (1)$$

The different terms in the right-hand side refer to horizontal transport ( $u$  is the horizontal velocity vector), thermodynamics ( $\theta$ ), and ridging and rafting ( $\psi$ ) (see Rousset et al., 2015). Technically, this equation reflects that each process affecting ice mass also affects DFe content, in a conservative manner, and that DFe content in sea ice (and in surface waters) is updated at each time step.

The specification of DFe incorporation and its functional dependencies on the sea-ice mass balance and ocean DFe deserve more attention. Several authors (Lancelot et al., 2009; Wang et al., 2014) have discussed these drivers since they ultimately control the DFe concentrations in sea ice. Let us first mention several overarching aspects. First, the amount of DFe incorporated into sea ice cannot exceed the total amount of DFe available in the underlying seawater. To prevent this to occur, we impose zero Fe flux for zero surface ocean concentration in Fe. Second, the incorporation of DFe is only effective during the formation of sea ice. Third, DFe in sea ice is released directly into surface seawater when sea ice melts.

Since little information is available to constrain a robust and unique description of the incorporation and release processes of DFe in and out of sea ice, we explored three plausible formulations relying on simple assumptions for the Fe incorporation into sea ice: CST, FLXCST, and FLXVAR (Table 1). In the CST formulation, DFe is taken from the first ocean level corresponding to a surface layer of 10 m in our configuration to achieve a constant and spatially uniform DFe concentration in sea ice of  $10 \text{ nmol L}^{-1}$ , our best estimate of the observational mean (Lannuzel et al., 2016), provided sufficient Fe stocks in the surface ocean. Such approach assumes an instantaneous equilibrium state between sea ice and seawater during the incorporation of DFe into sea ice. Iron incorporation is assumed infinitely fast compared to ice growth, and the Fe storage capacity of sea ice is instantaneously saturated. Such behavior would occur, in essence, for a rapid adsorption onto elements such as sea-ice crystals, organic matter, and brine inclusion surfaces, as suggested by Janssens et al. (2016), but is somehow inconsistent with an increase of DFe concentration with ice thickness. This parameterization is close to that of Lancelot et al. (2009), except for the prescribed DFe concentration they used ( $16.5 \text{ nmol L}^{-1}$ ), which was constrained by the observations available back then.

In the FLXCST formulation, we prescribe a constant DFe flux between seawater and sea ice, provided sufficient Fe stocks in the surface ocean. The value of the DFe flux was set to achieve a DFe concentration of  $10 \text{ nmol L}^{-1}$  in 1-m-thick sea ice over a 3-month period, a typical time scale for sea-ice growth in the SO (Worby et al., 2008). This corresponds to a finite Fe flux of  $1.3 \cdot 10^{-6} \text{ nmol m}^{-2} \text{ s}^{-1}$  (unlike the infinite flux assumed for the CST formulation). In this case, sea ice has an adsorption capacity that does not change or saturate and is thus potentially infinite (provided unlimited oceanic supply). Lannuzel et al. (2016) highlighted that DFe concentration increases with ice thickness (see their Figure 6), underlining a possible continuous pumping of seawater DFe into sea ice.

In the FLXVAR formulation, the Fe fluxes depend on DFe concentrations in surface seawater:

$$F_{Fe} = k \cdot DFe_w, \quad (2)$$

where  $k$  is a constant exchange velocity ( $4 \cdot 10^{-6} \text{ m s}^{-1}$  in the control case; see Table 1), the value of which was adjusted in the model to achieve an annual mean sea-ice DFe concentration close to  $10 \text{ nmol L}^{-1}$ . The FLXVAR formulation postulates a linear change in the rate of incorporation of DFe into sea ice as a function of the availability of DFe in surface seawater. This may be one of the main factors contributing to the observed variations of DFe in sea ice, the Fe content in sea ice tending to decrease with distance from the coast (Lannuzel et al., 2016). Similar to the FLXCST parameterization, the uptake capacity of sea ice is supposed to be large enough such as it is never approached in practice, that is, potentially infinite. This formulation is comparable to that of Wang et al. (2014), except that in their study, this fraction increases where sediments are shallower than 50 m.

One of the approximations we make in the model is that we assume a vertically constant Fe profile, which implies a continuous release of Fe upon melt. In reality, the release of Fe from melting sea ice could be more intense but shorter, because concentrations are much larger near the ice base and low elsewhere.

### 2.3. Experimental Design

To explore the implications of the different incorporation formulations, we designed seven experiments described in Table 1. All the experiments were run for 15 years in climatological conditions using the CORE-I normal year atmospheric forcing fields (Griffies et al., 2009). After 15 years, differences between the sensitivity experiments only evolve very slowly (Figure S1 in the supporting information). They are all initialized from the annual climatologies of the World Ocean Atlas 2013 for temperature (Locarnini et al., 2013) and salinity (Zweng et al., 2013), the World Ocean Atlas 2009 for nutrients (nitrate, phosphate, and silicate Garcia et al., 2010a), and oxygen (Garcia et al., 2010b) and GLODAP-v1 for DIC and alkalinity (Key et al., 2004). Iron is initialized from a previous simulation run to a quasi-steady state (the simulation presented in Aumont et al., 2015). The sea-ice state variables (thickness, concentration, salinity, and temperature) are set to constant values when sea surface temperature is lower than  $2^\circ\text{C}$  and sea-ice Fe is initialized to  $10 \text{ nmol L}^{-1}$  uniformly. These experiments were carried out under preindustrial atmospheric  $\text{CO}_2$  concentration conditions (280 ppm). Only the last year of the 15-year simulations is considered in the analysis of the results. In the CTL experiment, which is used as a reference, exchanges of DFe between sea ice and surface seawater are ignored, which means that there is no incorporation of DFe into sea ice and DFe concentration in sea ice is therefore zero. The CST, FLXCST, and FLXVAR experiments, respectively, adopt the three formulations of the incorporation of DFe into sea ice described in section 2.2. The FLXVAR2 experiment is identical to FLXVAR but with a two times higher exchange coefficient to evaluate the sensitivity of the model in the case of a stronger Fe flux between sea ice and seawater. In order to evaluate the contribution of the sediment Fe source to the sea-ice Fe reservoir in the case of a variable DFe flux (as suggested by de Jong et al., 2013), two additional experiments were designed: CTLnoSed and FLXVARnoSed. The parameterizations are the same as the CTL and FLXVAR experiments, except that the external source of sedimentary Fe is deactivated.

## 3. Results

### 3.1. The Simulated Ocean and Sea-Ice Environments and Iron Concentrations in Seawater

We first describe the physical behavior of our model using annual sea-ice growth and melt and mixed layer depth (MLD) seasonal changes (Figure 1), which both have a first-order impact on the Fe reservoir in sea ice. Sea-ice extent, as well as regions of sea-ice growth and melt, modulate the spatial distribution of Fe fertilization by sea ice. Seasonal MLD changes, particularly the fall and winter deepening, determine how much Fe is available at the ocean surface and therefore control the subsequent incorporation into sea ice.

Annual ice growth is the highest near the Antarctic coast, reflecting polynya activity, and decreases toward lower latitudes, vanishing at  $60^\circ\text{S}$  in the Atlantic and Indian sectors and at  $65^\circ\text{S}$  in the Pacific sector (Figure 1a). The spatial distribution of sea ice is different between melt and growth (Figure 1b), reflecting ice transport. The highest annual melt rates are found in the western Ross Sea, along the coasts of the Bellingshausen and Weddell Seas, and in coastal areas near Dronning Maud Land ( $0\text{--}50^\circ\text{E}$ ). Off East

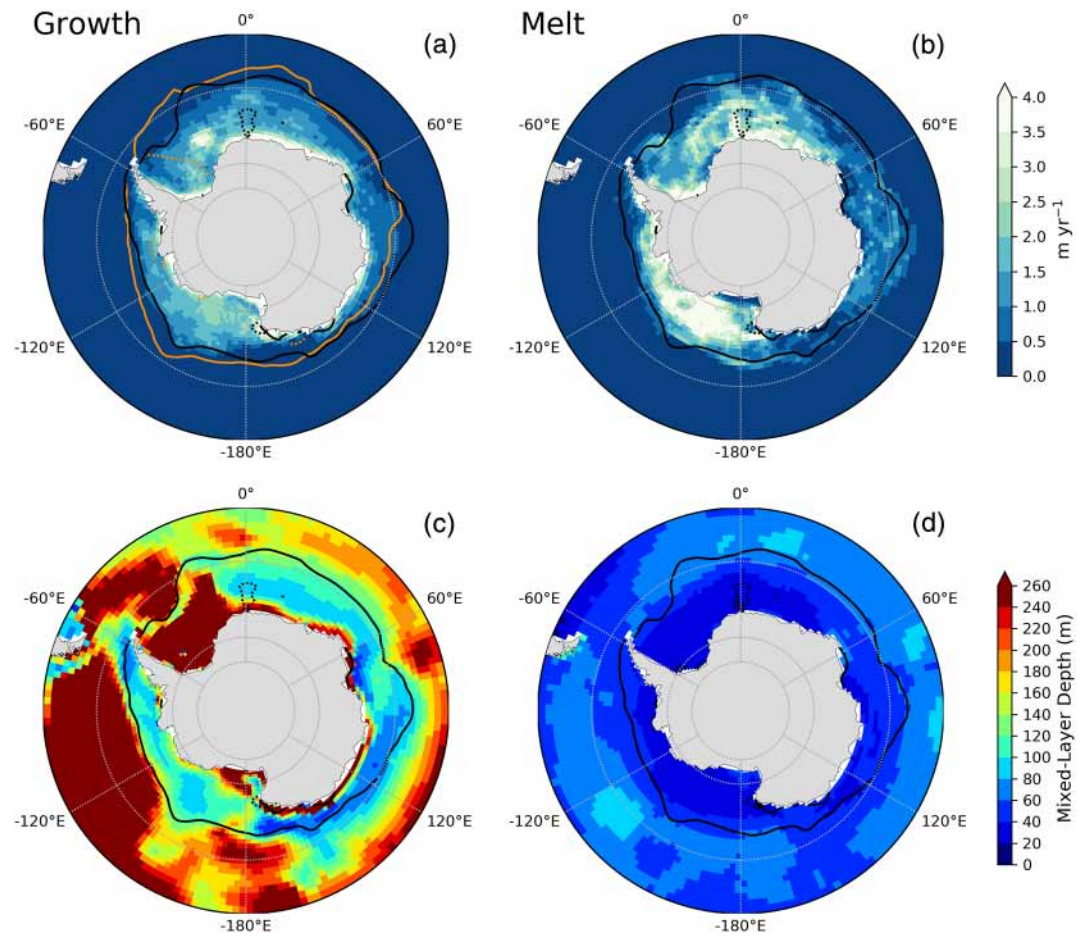


**Figure 1.** Annual sea-ice (a) growth and (b) melt, and mixed layer depth in (c) winter (June–August) and (d) summer (December–February) in the Southern Ocean simulated in the experiments (last year of the 15-year simulations). Black lines denote the model ice edge (15% ice concentration contour) in September (solid) and February (dotted). Corresponding satellite averages for the 2010–2019 period from the OSI-SAF-450 passive microwave ice concentration product are given in orange (Lavergne et al., 2019, panel a only).

Antarctica, Wilkes and Adélie Lands (60–160°E), sea ice melt is the lowest. The annual maximum sea-ice extent in September is fairly well simulated. An overestimation of the strength of the Antarctic circumpolar current in our configuration likely led to an under-representation of the observed sea-ice extent in the Weddell Sea and western Pacific (Figure 1a). In summer, sea-ice retreat is high, highlighting the large seasonal variations in sea-ice extent observed in the SO, with sea ice forming anew every year compared to the Arctic where sea ice generally persists for longer periods of time. However, the simulated retreat is too large compared to the observations in some areas, as demonstrated by the complete lack of simulated sea-ice cover in the Weddell Sea.

Figures 1c and 1d show MLD defined by a fixed density threshold of  $0.03 \text{ kg m}^{-3}$  (de Boyer Montégut et al., 2004). In winter, the model simulates large MLD variations from 60 to 260 m under sea ice (Figure 1c). Along the Antarctic coast, the mixed layer is deeper than 200 m consistent with polynya activity, as estimated in Pellichero et al. (2017). In the Weddell Sea, MLD is greater than 260 m, which could constitute a significant bias in our model, although mixed layers deeper than 200 m have also been reported from observation-based values (Pellichero et al., 2017). Note that the winter MLD simulated in the SO by the NEMO ocean model has recently been evaluated deeper than the observations (Person et al., 2018). MLD-sea ice relationships can be detected by visually comparing the upper and lower panels on Figure 1. Winter growth matches coastal MLD maxima, whereas the ice edge region is associated to sharp MLD

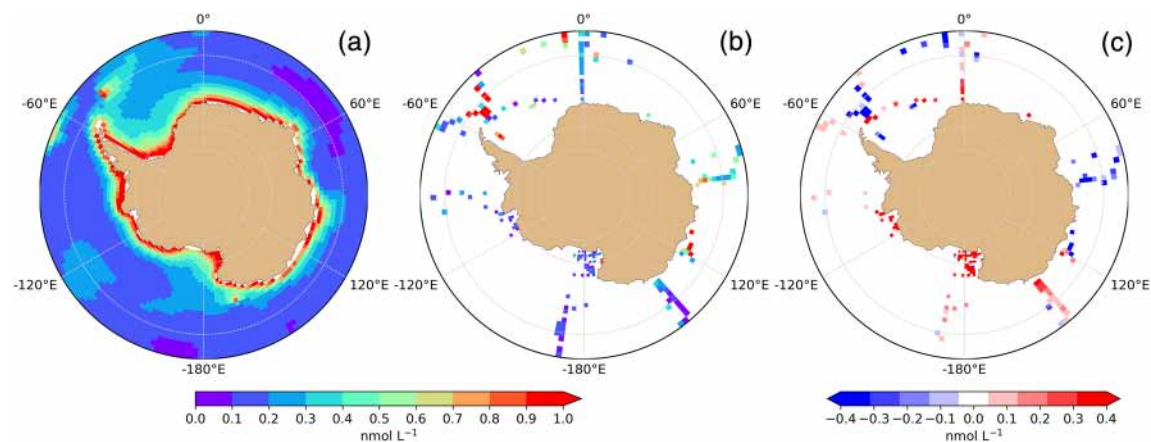


**Figure 2.** Annual seawater Fe concentrations averaged over 0–200 m in (a) the CTL experiment, (b) from observations (Tagliabue et al., 2012), and (c) difference between CTL and observations in the Southern Ocean, South of 55°S.

changes from low values under sea ice to high values in the open ocean. In summer, the upper ocean is generally stratified, more so in the presence of sea ice, and the spatial variations of MLD (20–60 m) are much weaker than in winter (Figure 1d).

Finally, we evaluate the distribution of DFe in the first 200 m of the ocean in the CTL experiment compared to the compiled observations of Tagliabue et al. (2012) augmented with additional data from IDP2017 (GEOTRACES Intermediate Data Product 2017, Schlitzer et al., 2018), which determines the amount of DFe that can be incorporated into sea ice during its formation (Figure 2). The model does not perfectly represent the observed distribution of DFe in the SO but captures its mean concentration of  $0.43 \text{ nmol L}^{-1}$  (Table S1). Statistical analysis of the distribution of DFe, south of 55°S, shows a correlation coefficient of 0.27 and a mean absolute error of  $0.34 \text{ nmol L}^{-1}$  (Table S1). In the CTL experiment, the annual mean DFe concentrations decreases from the coasts toward the open sea, illustrating the role of sedimentary iron input (Figure 2a). Iron concentrations in near-shore seawater are greater than  $0.9 \text{ nmol L}^{-1}$  and offshore concentrations range from 0.1 to  $0.4 \text{ nmol L}^{-1}$ . The difference in DFe concentrations between the model and the observations (Figure 1c) shows overestimated concentrations in the Ross and Bellingshausen Seas and along transects at 0°E and 145°E. The overestimation decreases offshore. Concentrations are underestimated between 60°E and 120°E and east of the Antarctic Peninsula.

### 3.2. Biogeochemical Impacts of the Different Parameterizations

We analyze in the section below the impacts of the three parameterizations of DFe incorporation into sea ice on DFe concentrations in sea ice and surface seawater, and on surface chlorophyll concentrations (Schl), with a focus on the SO.

#### 3.2.1. Iron in Sea Ice and Surface Waters

In the CST experiment, the spatial distribution of annual DFe concentrations in sea ice is completely homogeneous (Figure 3a), indicating that DFe in surface seawater is never exhausted during the growth phase of sea ice. Although surface DFe concentrations in the SO are low, the intense mixing and the vertical entrainment of DFe from subsurface waters into the mixed layer in fall and winter provide sufficient DFe to the surface layer of the ocean model to ensure a DFe concentration of  $10 \text{ nmol L}^{-1}$  in sea ice. That sea-ice DFe is spatially homogeneous in the CST simulation differs from the results of Lancelot et al. (2009), which show two large areas of very low sea-ice DFe concentrations east of the Weddell and Ross Seas (see their Figure 6b), despite the use of a parameterization similar to CST. This suggests a low DFe availability in surface waters during sea-ice formation. We speculate this to be due to the relatively shallow winter under-ice mixed layer simulated by their model, typically in the range of 40 to 80 m, whereas they are generally between 80 and 120 m in our model and deeper than 200 m in the Weddell Sea and along the Antarctic coast (Figure 1c).

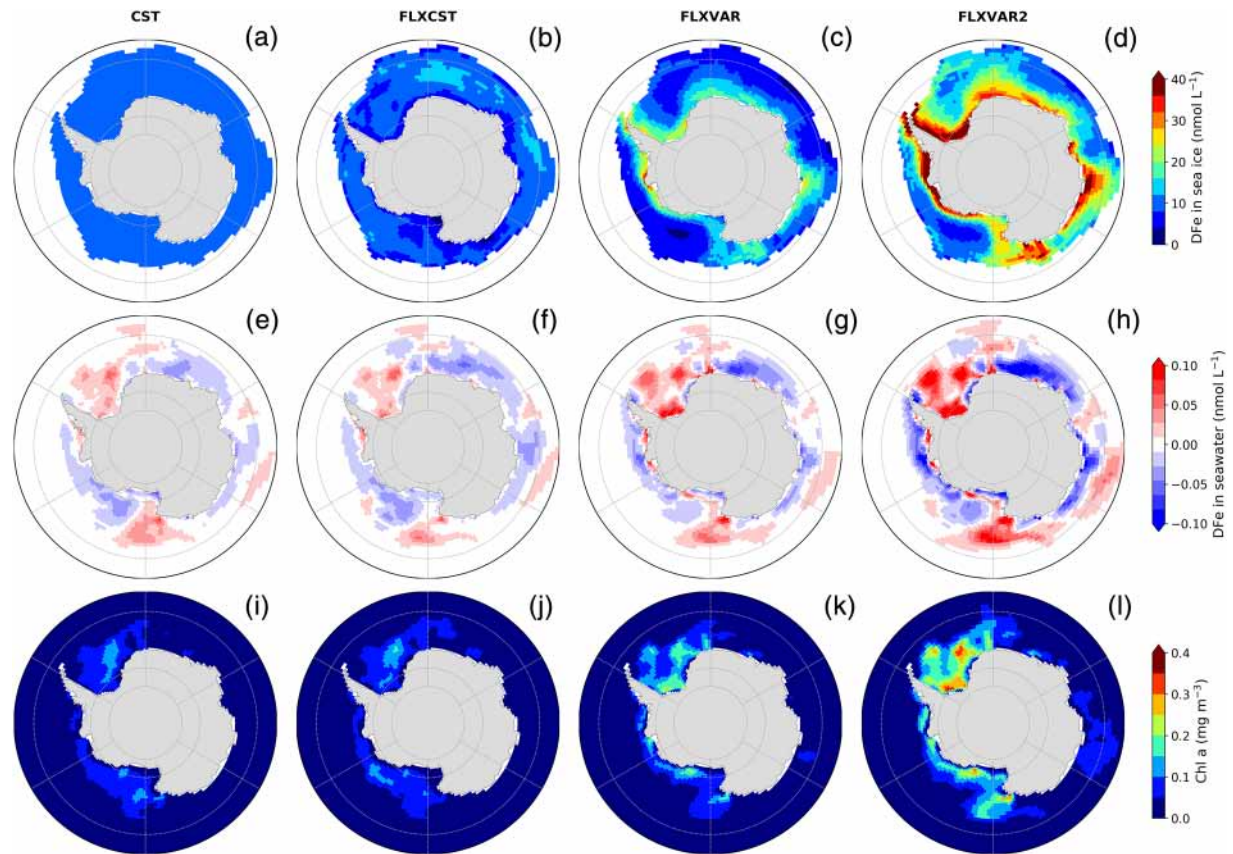


**Figure 3.** (a–d) Annual-mean DFe concentrations in sea ice and annual anomalies of (e–h) DFe and (i–l) chlorophyll concentrations in surface seawater in the different experiments (see Table 1) relative to the CTL experiment in the Southern Ocean, south of 50°S.

In the FLXCST experiment, the spatial distribution of DFe concentrations in sea ice is no longer homogeneous, with values ranging from 1.6 to 14.1  $\text{nmol L}^{-1}$ . The constant-flux parameterization induces a quasi-linear relationship between sea-ice DFe concentration and sea-ice age (not shown). The highest sea-ice DFe concentrations are simulated where the ice is the oldest, that is, in the open ocean regions of the Atlantic and Indian sectors. The lowest values are found near coastal polynyas, particularly in the Ross Sea (Figure 3b).

The FLXVAR and FLXVAR2 experiments assume that the ocean-ice DFe flux is a function of surface seawater DFe concentration, which induces a large increase in sea-ice DFe concentration as we move southward (Figures 3c and 3d), which is consistent with field observations (Lannuzel et al., 2016). The simulated DFe concentrations in sea ice range from 2.6 to 39  $\text{nmol L}^{-1}$  in FLXVAR and from 5 to 67.5  $\text{nmol L}^{-1}$  in FLXVAR2. Although the FLXVAR formulation is comparable to that proposed by Wang et al. (2014), FLXVAR gives a median sea-ice DFe concentration about an order of magnitude larger than in the Wang et al. study and a largely different spatial distribution. Indeed, in Wang et al. (2014), only the Bellingshausen Sea shows DFe concentrations in sea ice above 5  $\text{nmol L}^{-1}$ , whereas the rest of the Antarctic pack ice has values between 1 and 2  $\text{nmol L}^{-1}$ . We speculate the Wang et al. DFe values in sea ice to be due to a much weaker background incorporation coefficient and a strong but highly localized sediment incorporation near the Antarctic Peninsula, noting that their model was tuned for global (including Arctic) conditions.

In summary, we do find important differences in the spatial distribution of DFe in sea ice between the three formulations. However, changes in the incorporation pathways do not result in largely different surface seawater DFe concentrations (Figures 3e–3h; Table S1). The patterns of surface seawater DFe concentrations anomalies, referred to the CTL experiment, are very similar, with positive and negative values in similar



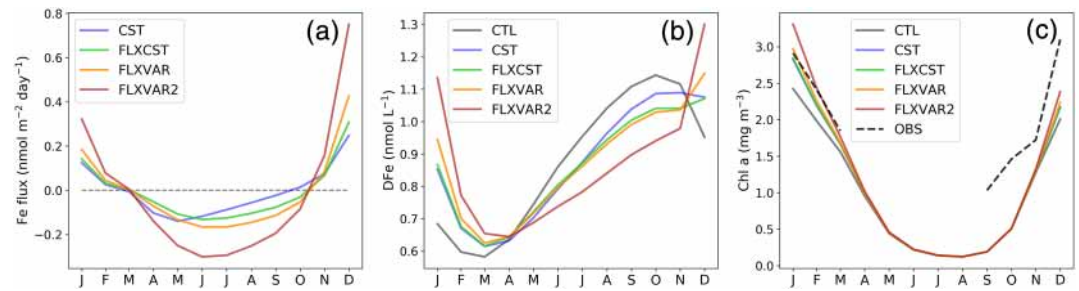


**Figure 4.** Seasonal cycles of (a) ice-to-ocean Fe flux and surface seawater (b) DFe and (c) chlorophyll concentrations, for the different experiments (see Table 1) in the Southern Ocean, south of 65°S. Satellite observations (MODIS Aqua; Johnson et al., 2013) are given in panel (c).

regions. The most notable differences are larger contrasts in seawater DFe concentration anomalies in FLXVAR compared to the CST and FLXCST experiments, contrasts that are even more pronounced in FLXVAR2. Regions showing larger surface seawater DFe concentrations are located in the Weddell and Ross Seas and off East Antarctica between 90°E and 120°E. In the FLXVAR and FLXVAR2 experiments, increased DFe concentrations in seawater also occur along the Antarctic coast from the Ross Sea to the Bellingshausen Sea (Figures 3g and 3h).

### 3.2.2. Chlorophyll in Surface Waters

The release of DFe from sea ice into surface seawater leads to positive anomalies of surface chlorophyll mostly in the western sector of the SO (Figures 3i–3l), corresponding to the areas with the highest seawater DFe anomalies (Figures 3e–3h). The distribution of surface chlorophyll anomalies in the sensitivity experiments, relative to the CTL experiment, is significantly correlated to sea-ice age ( $r = 0.80$ ) and thickness ( $r = 0.78$ ). The Fe supply from sea ice in this region increases annual SCHl by up to  $0.15 \text{ mg m}^{-3}$  in CST,  $0.2 \text{ mg m}^{-3}$  in FLXCST,  $0.25 \text{ mg m}^{-3}$  in FLXVAR, and  $0.4 \text{ mg m}^{-3}$  in FLXVAR2. The strength of the Fe fertilization by sea ice is relatively modest but spatially extensive at the scale of the SO. The regions mainly impacted are the Weddell and Ross Seas in all experiments and the coastal regions between the Ross and Bellingshausen Seas in the FLXVAR and FLXVAR2 experiments.

### 3.2.3. Seasonality of the Impacts of Iron Incorporation Into Sea Ice

We now turn to the results of the impacts of Fe incorporation into sea ice on the seasonal time scale (Figure 4). The seasonal cycles of the ice-ocean Fe flux are similar between the CST, FLXCST, and FLXVAR experiments (Figure 4a). The FLXVAR2 experiment simulates the largest amplitude of the seasonal exchange of DFe between sea ice and seawater, which leads to an important DFe supply to seawater from November to January. The storage and release of DFe in and from sea ice modify the seasonal evolution of the surface DFe concentrations relative to the CTL experiment (Figure 4b). The maximum DFe supply, which occurs in October in CTL, arises 2 months later, in December, in FLXCST and FLXVAR, and is particularly marked in FLXVAR2. The increase in surface DFe concentrations in January ranges from  $0.2$  to  $0.4 \text{ nmol L}^{-1}$  in the sensitivity experiments compared to CTL. For SCHl, the fertilization effect of sea ice increases the maximum bloom values in January by  $0.4$  to  $0.8 \text{ mg m}^{-3}$  in the four experiments relative to CTL (Figure 4c). This increase slightly improves the amplitude of the SCHl seasonal cycle from November to March relative to the observations in the seasonal ice zone. However, the timing of the phytoplankton bloom peak that occurs on average in December in the data is still not well reproduced by the experiments, which simulate a later bloom peak in January. The impacts of sea ice on the seasonal cycle of surface Fe in our experiments suggest that the role of melting sea ice may not act as a “pulsed source of Fe,” that is, a short-term supply of Fe as proposed by Lannuzel et al. (2016), but rather as a relatively sustained supply from November to January for phytoplankton activity.

### 3.3. Ice-Ocean Iron Fluxes

One result from the previous section that deserves further investigation is the insensitivity of the spatial distribution of surface DFe anomalies in seawater driven by the ocean-to-sea-ice incorporation pathways (Figures 3e–3h). We argue that this is due to the sea-ice Fe uptake, transport, and release mechanisms, already mentioned by Lancelot et al. (2009), whose effects dominate the details of the Fe incorporation formulation.

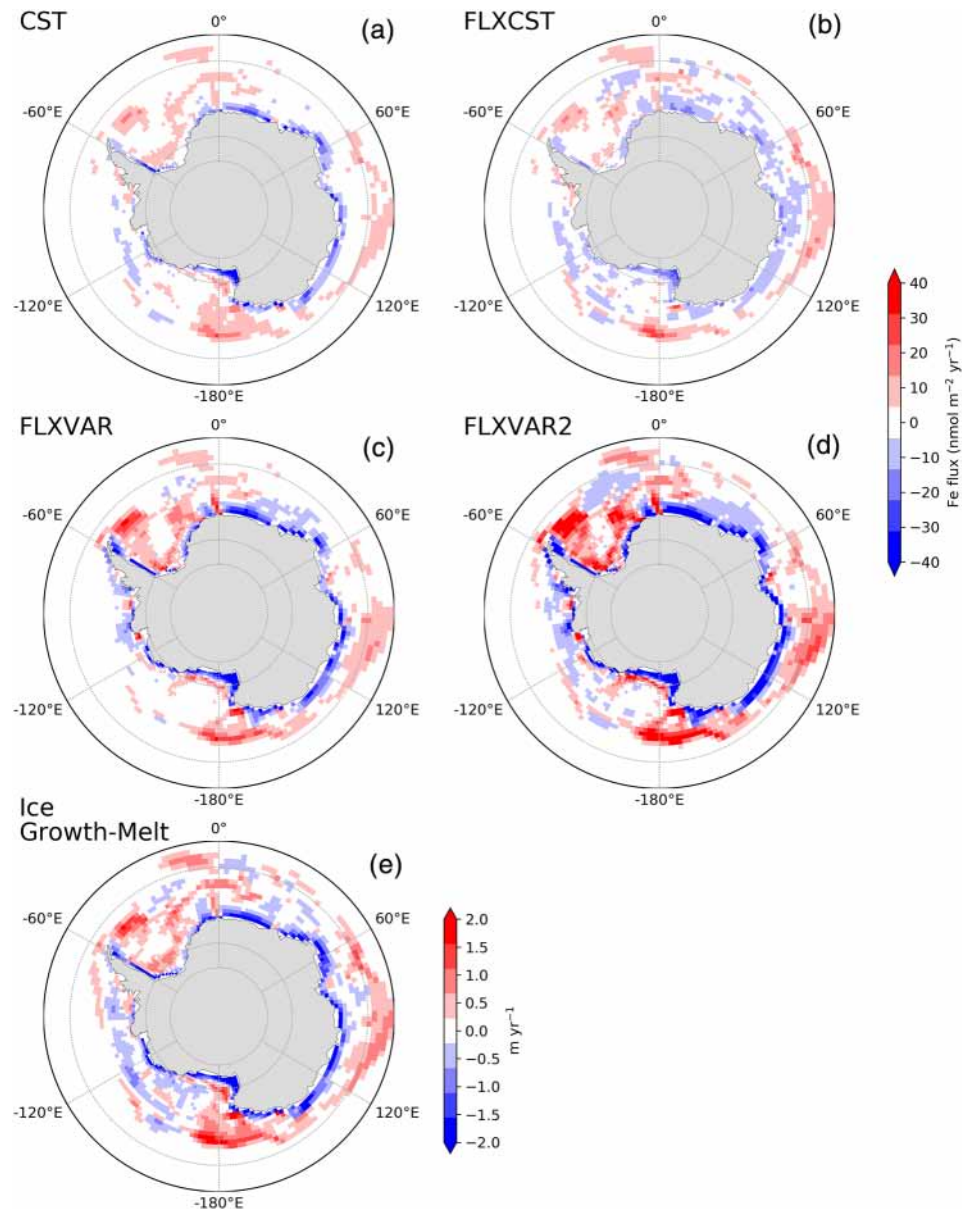


**Figure 5.** (a–d) Annual ice-to-ocean Fe flux in the different sensitivity experiments (see Table 1) and (e) net annual ice growth and melt (same for all sensitivity experiments).

All Fe incorporation parameterizations assume Fe incorporation into sea ice during freezing and release when sea ice melts. This induces the strong relationship found between annual mean ice-ocean Fe fluxes and net annual ice growth and melt, obvious in Figures 5a–5d. The strength of the relationship varies between simulations but is in all cases rather high, as highlighted by high correlations between variables (Table S2). In the CST experiment, the correlation coefficient is close to 1, because a linear relationship between the ice-ocean Fe flux and net sea-ice growth and melt rate is enforced by construction. In the FLXCST experiment, the correlation is the weakest ( $\sim 0.7$ ), because in this case only the sign of the Fe flux relates to ice growth and melt, whereas the magnitude of the flux is constant. The variable flux experiments show a stronger relationship than in FLXCST (correlation  $\sim 0.8$ ), due to the spatial coincidence of sea-ice formation sites and the regions of highest DFe seawater concentrations, as a consequence of the Fe input from sediments in coastal regions.

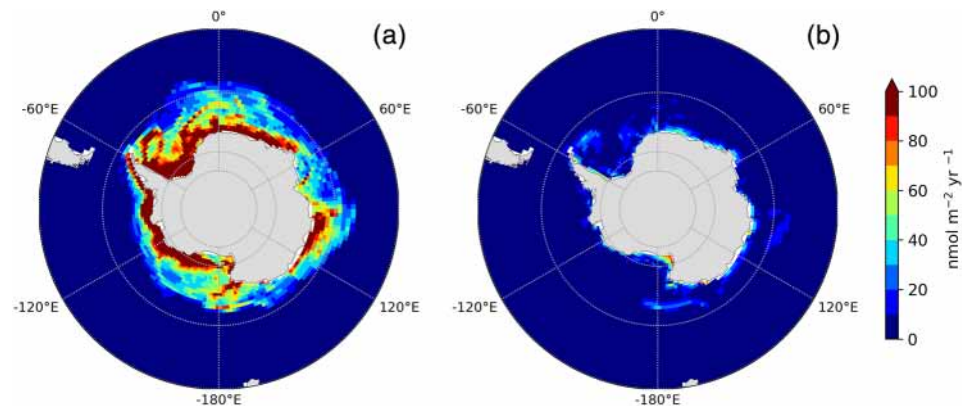


**Figure 6.** Ice-ocean Fe flux in the FLXVAR experiment: (a) amplitude of the seasonal cycle (half of the maximum-minimum difference for a periodic signal) and (b) annual mean value.

The difference between growth and melt locations is due to ice transport. Hence, the link between Fe flux anomalies and ice growth and melt suggests the role of Fe uptake, transport, and release by sea ice. This mechanism relies upon the uptake of a sufficient load of Fe in forming sea ice, rather than on the exact dependence of Fe uptake on sea-ice growth rate, and is reinforced by the coastal sedimentary source of DFe. The ice forming preferentially near the coast is iron laden, then drifts to the north and releases its Fe stock where it melts, relatively far from the coastal regions, as shown by the large positive values in the Weddell and Ross Seas and in the offshore region between 60°E and 120°E (Figure 5e).

### 3.4. Ice Thermodynamics and Dynamics Contribution to Ice-Ocean Iron fluxes

Ice transport shapes the spatial response of ice-ocean fluxes to the Fe incorporation formulation. Whether ice transport is also an important driver of the seasonal cycle of ice-ocean Fe fluxes is a different question. We investigate this by looking at ice-ocean Fe fluxes and their seasonal cycle (Figure 6), using the FLXVAR experiment as the most plausible scenario, noting that this framework is applicable to all experiments.

The seasonal cycle of the ice-ocean Fe flux is characterized by an uptake during the ice growth season and by a release during the melt season. In most locations, incorporation and release compensate for each other. In such regions, the effect of ice growth and melt (thermodynamics) dominates, and the annual mean ice-ocean Fe flux is close to zero (Figure 6b).

Where the annual mean ice-ocean Fe flux significantly departs from zero indicates a net Fe transport into or out of the region, highlighting the role of Fe transport by ice dynamics. Such regions include the coastal, shallow regions, where the net Fe flux into the ice is comparable in magnitude or higher to the amplitude of the seasonal cycle. This seems particularly the case near coastal polynyas (Ross Sea and East Antarctica), and somehow in the most important melting regions, in the north western Ross Sea, east of the tip of the Antarctic Peninsula, and off East Antarctica.

### 3.5. Observational Constraints on Iron in Sea Ice

How plausible are the different formulations of Fe incorporation into sea ice? Observations are under-sampled in space and time. Therefore, a spatiotemporal model-observation comparison would not be helpful. Possibly more informative are the relationships between Fe concentrations in sea ice and thickness and bathymetry (Figures 7 and 8, which can be inferred from observations Lannuzel et al., 2016). To test how the latter are simulated, we used the 56 Antarctic sea-ice cores with dissolved Fe data from the compilation of Lannuzel et al. (2016). The evaluation was performed in spring (September–November), when observations are the most abundant. As there is a tendency to sample thin and undeformed ice, there is a presumed low ice thickness bias in the data set and very few data points with thickness larger than 1 m.

#### 3.5.1. Iron in Sea Ice and Ice Thickness

We first examine the simulated range of DFe concentrations in sea ice, which lied between 0 and 45 nmol L<sup>-1</sup> in the observations. In the CST experiment, as expected, there is no variation in DFe

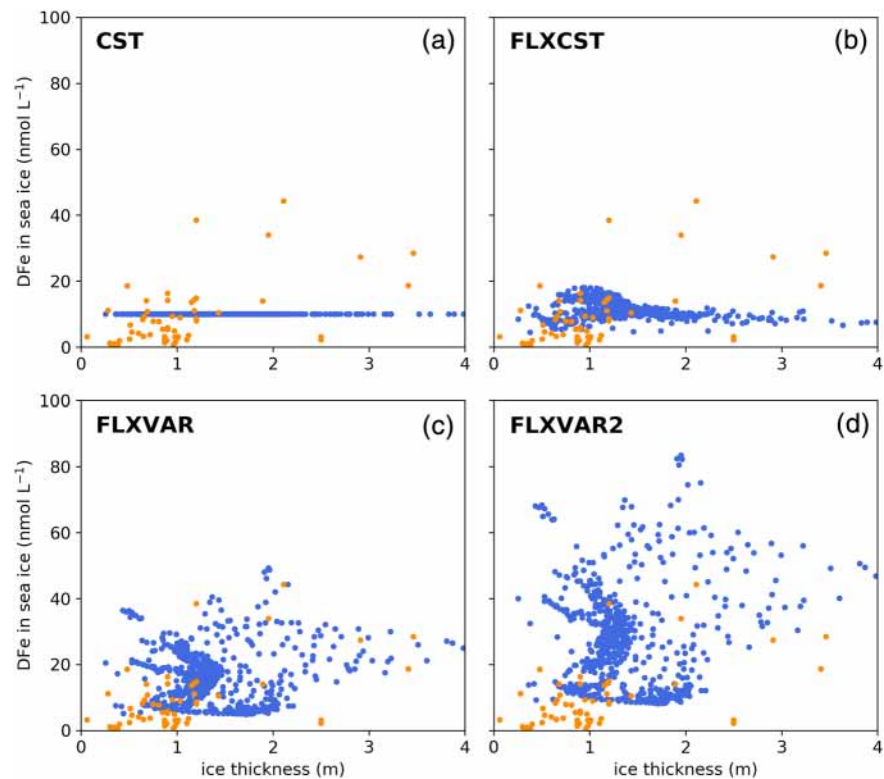


**Figure 7.** (a–d) Vertically averaged DFe concentration ( $\text{nmol L}^{-1}$ ) in sea ice versus thickness, drawn from the different sensitivity experiments (blue dots; see Table 1) and observations from Lannuzel et al. (2016) (orange dots). The comparison to observations concerns the model's spring (September–November) data over the entire sea-ice cover, season when a large part of the data is acquired. Ice thickness is identical among the different experiments.

concentrations in sea ice relative to thickness (Figure 7a), which is in sharp contrast with observations. FLXCST simulates sea-ice DFe concentrations in the  $4\text{--}20\text{ nmol L}^{-1}$  range, corresponding to the 0.5- to 1.5-m ice thickness range (Figure 7b), in reasonable agreement with observations, except for the few extreme values above  $20\text{ nmol L}^{-1}$  and the lowest concentrations below  $4\text{ nmol L}^{-1}$ . The FLXVAR experiment simulates a wider range of DFe concentrations in sea ice, from 4 to  $45\text{ nmol L}^{-1}$ . This formulation reproduces well the highest observed values (Figure 7c), however still missing the lowermost values. FLXVAR2 amplifies the simulated variability of DFe concentration in sea ice with maxima twice as high as observed, and no longer representing values within the  $4\text{--}10\text{ nmol L}^{-1}$  range (Figure 7d). This simulation contrasts with field observations. In short, there are differences in the simulated range of DFe concentrations in sea ice, and FLXVAR arguably produces the outputs the closest to field observations. However, none of the formulations fully capture observations, in particular for the lowest values.

Now we turn to the key statistics of the simulated distributions of DFe content in sea ice, for the month of November (Table 2). This evidences that the different parameterizations do not fully capture the observed distribution. FLXVAR2 has the closest mean to observations, whereas it is underestimated in the CST, FLXCST, and FLXVAR experiments. FLXVAR and FLXVAR2 simulate a higher variance in better agreement with the observations. Moreover, the median is overestimated in all experiments. Finally, the interquartile range is fairly well captured in the CST and FLXCST experiments but is too high in FLXVAR and FLXVAR2. That no simulation is able to capture all these statistics together suggests that important processes are not properly represented or are missing in the model.

### 3.5.2. Iron in Sea Ice and Water Depth

Observations suggest an inverse relationship between the DFe content in sea ice and the water column depth (Lannuzel et al., 2016), which we explored in the different sensitivity experiments (Figure 8). Such relationship is understood as the result of two factors (de Jong et al., 2013; Lannuzel et al., 2016). First, near the coast,

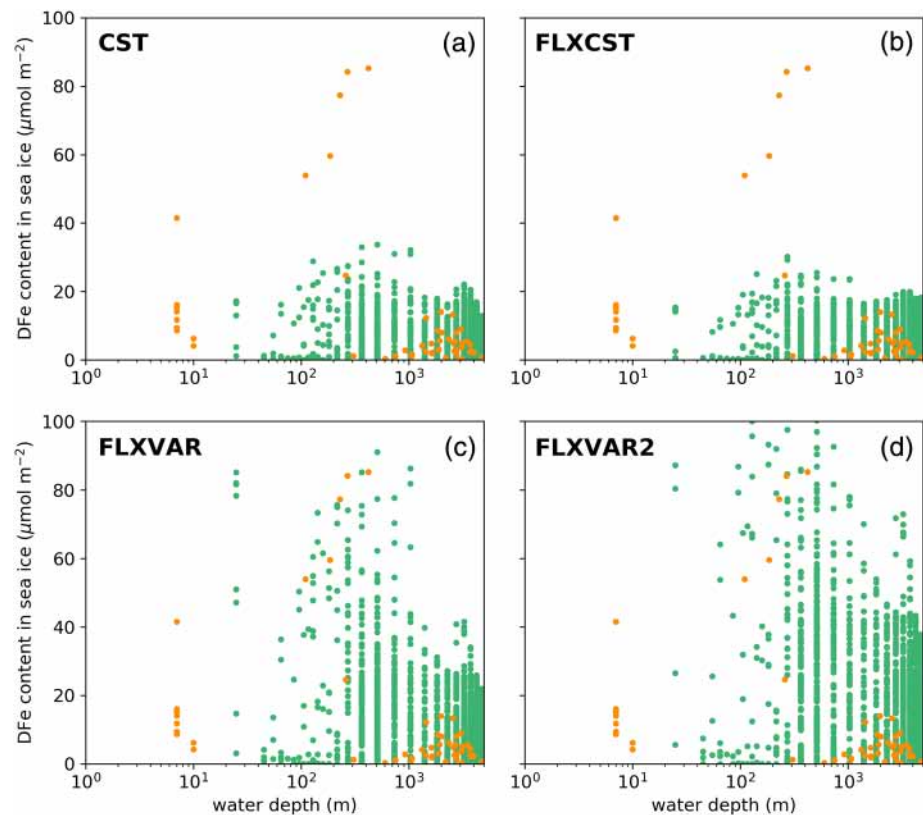


**Figure 8.** (a–d) Vertically averaged DFe content ( $\mu\text{mol m}^{-2}$ ) in sea ice versus water depth, taken in the different sensitivity experiments (green dots; see Table 1) and observations from Lannuzel et al. (2016) (orange dots). The comparison to observations concerns the model’s spring (September–November) data over the entire sea-ice cover, season when a large part of the data is acquired. Water column depth is identical among the different experiments.

the sedimentary and coastal Fe sources are the largest. Second, sea ice attached to the coast is typically landfast, that is, immobile for most of the growing season (Fraser et al., 2012), inducing an exposure to iron-rich coastal waters for at least 6 months. By contrast, the drifting pack ice, found further offshore, travels several hundreds of kilometers every month.

A relationship between Fe content and water depth is hardly simulated in our experiments, in particular in the CST and FLXCST experiments, a bit less so in FLXVAR and FLXVAR2. A first reason to this deficiency is the absence of Antarctic fast ice in our model, a shortcoming of the current generation of sea-ice models. Therefore, the long exposure times to iron-rich coastal waters are not represented. In the observational data set, all points with the largest Fe contents (above  $40 \mu\text{mol m}^{-2}$ ) have been measured in landfast ice, corresponding to depths up to about 200 m. Note that water depth is cut off at 25 m in our model configuration; hence, the very shallow waters (<10 m) can be considered as equivalent to depths of 25 m.

**Table 2**

Summary Statistics for Dissolved Fe Content in Antarctic Sea Ice ( $\mu\text{mol m}^{-2}$ ), in November, Month When Observations Are Most Abundant (Lannuzel et al., 2016), From the Different Sensitivity Experiments (See Table 1)

	Observations	CST	FLXCST	FLXVAR	FLXVAR2
Mean $\pm$ STD	$12 \pm 20.4$	$6.2 \pm 5.6$	$6.4 \pm 5.7$	$7.7 \pm 14.2$	$13.8 \pm 25.4$
Median $\pm$ IQR	$4.7 \pm 7.8$	$8.3 \pm 7.3$	$10.2 \pm 9.3$	$10.7 \pm 14.1$	$18.8 \pm 24.5$

Note. Statistics are calculated over the entire sea-ice cover for the modeling experiments and from the 56 ice cores available for observations. STD = standard deviation; IQR = interquartile range.

The variable Fe flux formulation (Figures 8c and 8d) responds to the iron-rich coastal waters and therefore generates a northward decrease of Fe content, which can be deemed as somehow realistic. However, at greater depths, the Fe content is overestimated by a factor of 2 and 3 in FLXVAR and FLXVAR2, respectively.

## 4. Discussion

Now we turn to the discussion of the implications of our results, in terms of Fe incorporation into sea ice and synergies with sediments, as well as on the large-scale drivers of Fe in sea ice and the associated uncertainties. Finally, we also discuss the impacts of sea-ice Fe transport on large-scale primary production and export.

### 4.1. Is There a Best Formulation for Iron Incorporation into Sea Ice?

Several formulations for the incorporation of Fe into sea ice have been previously proposed (Lancelot et al., 2009; Wadley et al., 2014; Wang et al., 2014). In light of our results, none of these approaches seem capable of capturing all aspects of the incorporation, transport, and release of Fe from sea ice. We showed that the ocean biogeochemistry is less sensitive to the mechanism of the Fe incorporation formulation than to the amount of DFe incorporated into and released from sea ice. From this point of view, the three formulations simulate sufficient and mutually consistent incorporation and release of DFe. However, with respect to the spatial distribution of Fe in sea ice, the variable Fe flux formulation (FLXVAR) seems the most suitable approach.

Imposing a constant DFe concentration in sea ice in the CST formulation assumes an instant saturation in sea ice. The continuous enrichment of DFe in young sea ice in the study of Janssens et al. (2016) suggests that, aside from rapid processes such as ice nucleation or scavenging by frazil crystals, other processes also important for the incorporation of DFe into sea ice such as the role played by extracellular polymeric substances and particulate organic carbon (Janssens et al., 2018) are not accounted for by this very simplified approach. In addition, the reported variations in DFe concentrations in sea ice (de Jong et al., 2013, 2015; Lannuzel et al., 2007, 2008, 2011, 2016; van der Merwe et al., 2011) strongly suggest that there is no saturation of the Fe storage capacity of sea ice as long as enough organic ligands are present to keep Fe in the dissolved phase. The observed non-uniform Fe distribution in sea ice underscores the inconsistency of the CST formulation in simulating the DFe variations in sea ice as a function of ice thickness as shown in Figure 7.

In the formulation specifying a constant flux of DFe (FLXCST), unlike the CST parameterization, the incorporation of DFe is not instantaneous. Sea ice can consistently incorporate as much DFe as possible if it is available in the surface seawater during its growth phase. This assumption is more consistent with the continuous incorporation of DFe in young sea ice as shown by Janssens et al. (2016). However, this formulation also assumes that sea ice has an unchanging and uniform incorporation capacity, that is, the factors contributing to this incorporation do not affect the variability of the ocean-to-sea ice exchanges of DFe. This assumption is more difficult to justify. Sea ice is a very heterogeneous medium compared to seawater, a heterogeneity that could strongly influence the rate of DFe incorporation and the variance of the DFe content in sea ice. A less speculative discriminatory aspect is that the FLXCST parameterization fails to represent the decrease of DFe concentration in sea ice from the continental shelf to deep water regions (Lannuzel et al., 2016), which suggests that DFe concentrations in seawater could play a role.

In the variable Fe flux formulation (FLXVAR), we introduce a possible modulation of the incorporation rate of DFe in sea ice by the DFe concentration in seawater. Although this formulation is also quite simplistic, the FLXVAR parameterization simulates the steep gradient of DFe concentration in sea ice from coastal to open water, as well as the range of DFe concentrations in sea ice as a function of sea-ice thickness observed in the field. This parameterization is currently the best compromise to represent the spatial distribution and variance of the mean content of the sea-ice DFe reservoir in our model. The lack of knowledge about the processes that control the exchange of Fe between sea ice and the underlying seawater prevents the development of a more substantiated parameterization. Among the physical sources of uncertainties, let us mention the vertical transport by frazil ice in the water column, and by brine convection and percolation within sea ice. Biological and chemical processes arguably carry the largest uncertainties. Indeed, the

complexation of Fe by organic ligands, the uptake and remineralization by microbial organisms, and the adsorption of Fe onto ice crystals and biofilms are all suspected to contribute but are poorly understood (Lannuzel et al., 2016).

#### 4.2. Iron Transport by Sea Ice: A Control by Sediments

Prior to this study, it has already been argued that Fe incorporation during growth, transport by drifting ice and subsequent melting carries Fe from coastal regions to waters influenced by melting sea ice, remote from the coasts (Lancelot et al., 2009), which is confirmed by our study. Here, we additionally find that in our most plausible incorporation formulation (FLXVAR), Fe transport by sea ice is tightly linked to coastal sediments. Indeed, formulating Fe incorporation into sea ice as a function of surface seawater concentrations enhances Fe incorporation into sea ice in coastal areas. Two additional experiments with the deactivated sediment source, FLXVARnoSED and CTLnoSED, illustrate this (Figure 9).

FLXVARnoSED highlights the important link between the sediment Fe source and the sea-ice reservoir of Fe. Iron concentrations in sea ice are lower by a factor of about 2 without a sediment Fe source in FLXVARnoSED, as compared to FLXVAR (Figures 9a and 9b). The sharp northward decrease in Fe in FLXVAR nearly disappears in FLXVARnoSED, and ice-ocean Fe fluxes decrease by about 2. More generally, the influence of sea ice in the annual supply of DFe to surface waters remotely from the coast is largely reduced in FLXVARnoSed relative to FLXVAR (Figures 9c and 9d), particularly in the Weddell and Ross Seas regions, and off East Antarctica. In turn, when not incorporated and transported by sea ice, sediments can no longer have a very large and remote impact on surface water DFe concentrations. Conversely, Fe transport by sea ice is inefficient in the absence of sediments, as illustrated by the rather weak changes in DFe supply to surface seawater in FLXVARnoSed compared to CTLnoSed (Figure 9f).

This analysis highlights the key role of sediments on the Fe storage capacity of sea ice, consistent with findings from Lannuzel et al. (2016) and Lancelot et al. (2009). It also reveals that Antarctic coastal areas which combine an active formation of sea ice with the high availability of sedimentary Fe work in synergy to distribute Fe at the scale of the SO.

#### 4.3. Iron in Sea Ice: Large-Scale Processes and Uncertainties

We identified several key large-scale drivers for Fe in sea ice: Fe source and sink processes, as well as ocean and sea-ice characteristics. These drivers also likely provide the largest uncertainty sources of processes that control the incorporation of Fe into sea ice and its Fe content.

Iron incorporation into sea ice is key, but the underlying processes remain largely misunderstood and difficult to formulate properly. In addition, many other Fe source and sink processes are missing from the model. A clear illustration of this is the systematic inability of the model to simulate the observed low Fe concentration values in sea ice, pointing toward missing Fe sinks. There are lots of other possible absent processes that undermine the model ability to correctly simulate Fe in sea ice. Such processes are reviewed in Janssens et al. (2016) and Lannuzel et al. (2016) and, to name a few, include predominantly physical (brine dynamics and harvesting of frazil crystals), chemical (size distribution of Fe species, and adsorption and interactions with organic matter), and biological processes (autotrophic and heterotrophic activity).

The simulation of Fe processes in the Antarctic sea-ice zone also suffers from issues in the simulated hydrography. As an illustration, let us mention the differences in simulated Fe concentrations in sea ice between the CST parameterization and the study of Lancelot et al. (2009), despite both approaches using very similar parameterizations of Fe incorporation into sea ice. The origin of these differences is likely associated with the depth of the mixed layer, about twice as deep in our study than in Lancelot et al. (2009). That MLD would affect Fe in sea ice makes sense: Mixed layer deepening sets the entrainment of subsurface Fe into surface water and availability for incorporation into sea ice. This would ultimately point toward differences in vertical mixing parameterizations, or in freshwater budget. It is beyond our scope to study the role of vertical mixing on Fe concentrations in sea ice, but we suspect that vertical mixing modulates Fe content in sea ice and hence is also an important source of uncertainty. Indeed, mixed layer in the SO is notoriously uncertain within ocean models, particularly under sea ice, which is most visible in climate simulations (Sallee et al., 2013). Recently, the ocean model NEMO that we use here was evaluated to simulate MLD in the

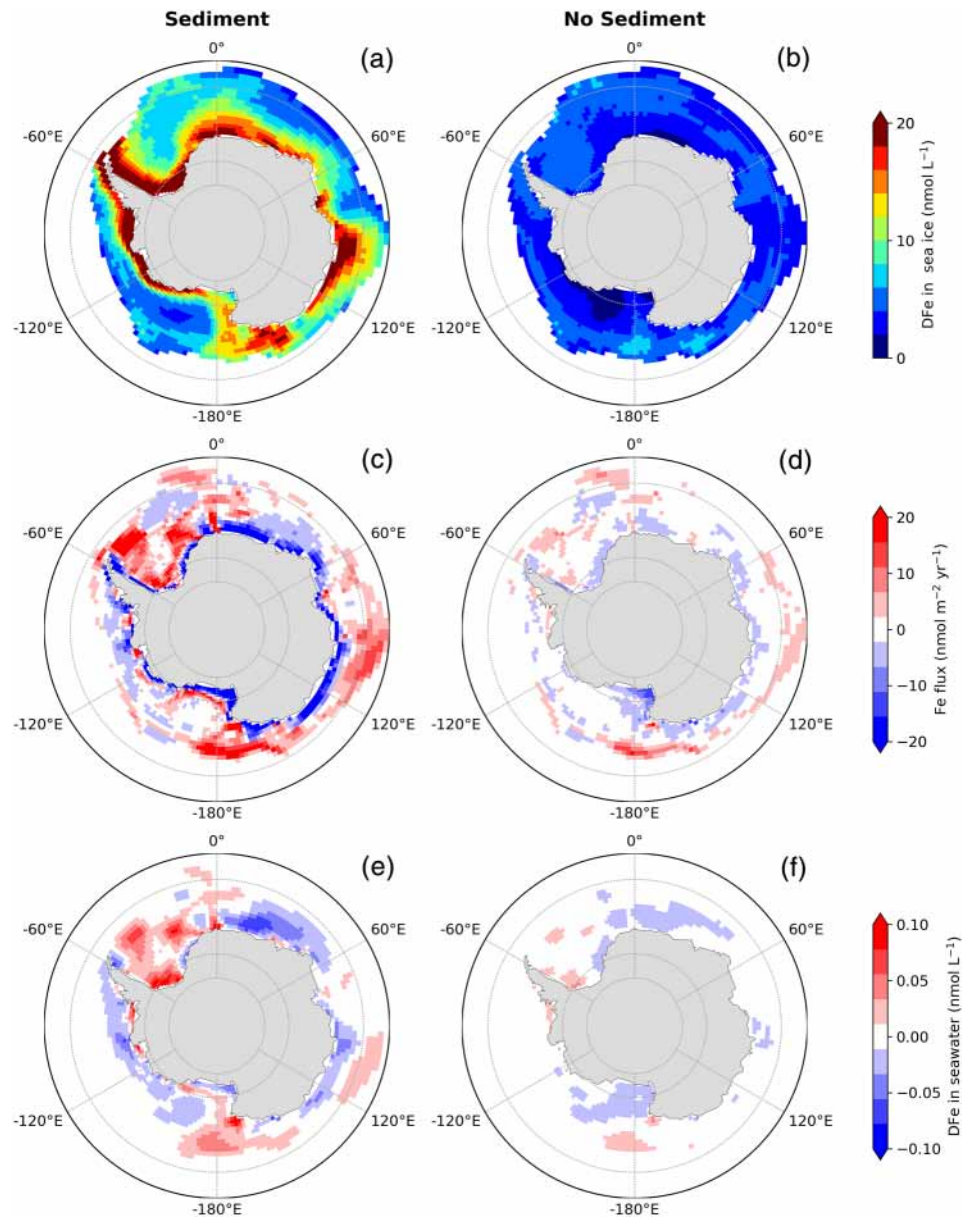


**Figure 9.** Role of the sedimentary Fe source, explored for the case of an ocean-ice DFe flux depending on surface ocean DFe concentration, highlighted by comparing the FLXVAR (left) and FLXVARnoSed (right) experiments: (a and b) DFe concentrations in sea ice, (c and d) ice-ocean Fe flux, and (e and f) anomalies of surface seawater DFe in seawater compared to the CTL and CTLnoSed experiments. All values are annual means.

SO that is systematically shallower in summer and deeper in winter (Person et al., 2018). Hence, winter entrainment of DFe in the mixed layer could well be overestimated in this study.

Observations and our simulations also stress ice thickness and landfast ice presence as particularly relevant to the Fe distribution in sea ice. First, observations as well as our most credible simulations support the relationship where the concentration of Fe in sea ice increases with ice thickness. An issue is that the simulated ice thickness suffers from the lack of reliable Antarctic sea-ice thickness estimates for baseline evaluation. Finally, a key aspect emerging from observations is the much larger Fe concentrations in landfast ice than in pack ice (Lannuzel et al., 2016). However, current sea-ice models are unable to simulate Antarctic landfast sea ice. These models have recently improved in the Arctic in that respect (Lemieux et al., 2016, 2018). However, as compared with the Arctic, Antarctic landfast ice is driven by specific processes that are



**Table 3**  
Annual Depth-Integrated Primary Production (PP) and C Export at 150-m Depth in the Different Experiments (See Table 1) and Associated Increase Relative to CTL (%)

	CTL	CST	FLXCST	FLXVAR	FLXVAR2
PP (TgC year <sup>-1</sup> )	759	799	801	808	839
PP change (%)		5.3	5.5	6.3	10.4
C export (TgC year <sup>-1</sup> )	218	236	237	242	259
C export change (%)		8.6	8.9	11.1	18.7

*Note.* Values are calculated over the September sea-ice cover area of the Southern Ocean and when the sea-ice concentration is at least greater than 15%.

currently unresolved in models (Fraser et al., 2012). Because of the absence of landfast ice, the long exposure times of landfast sea ice to iron-rich coastal waters are not represented in our model, which could bias the comparison between the different Fe formulations. Observations in sea ice zones remain the ultimate knowledge bottleneck, and better observational constraints on the relationships between ice thickness and Fe covering the whole range of observed sea ice thicknesses, or between latitude and Fe in sea ice would help to discriminate between the different Fe incorporation formulations. This could take the form of intense sampling of ice of widely different thicknesses at a similar location and time in the season. Transects over a few meridians, with a few cores taken every 1° or 2° of latitude, would also be useful.

Our study also overlooks the continental glacial inputs of Fe: The external source of Fe from icebergs and ice shelves is not included, which represents a potentially important Fe reservoir in the SO (Hopwood et al., 2019; Laufkötter et al., 2018; Person et al., 2019; Raiswell et al., 2016). Synergies between melting icebergs-ice shelves and incorporation in growing sea ice could occur, leading to increased Fe transport by sea ice, particularly in the coastal regions of Antarctica, and changing its distribution throughout the SO. This stresses out the need to consider both sea ice and continental ice Fe sources in future modeling studies.

#### 4.4. Should Primary Production and Carbon Export Estimates Be Revised in the Southern Ocean?

The distribution of Fe in sea ice remains challenging to understand and largely uncertain. Our results however suggest that the Fe fertilization effect on surface waters by sea ice is not as uncertain since it seems to be insensitive to the details of the formulation of Fe incorporation into sea ice. In light of this, we calculated the contribution of Fe in sea ice to primary production and carbon export at the scale of the SO. Only very few studies have addressed so far that contribution. Wadley et al. (2014) estimated the contribution of Fe in sea ice to SO primary production to 11%, which is significantly lower than their 75% estimated for the sedimentary Fe source. For C export, a contribution of sea ice of less than 4% is estimated in the SO (Wang et al., 2014), which falls within the 1–30% range of the contribution estimated for the iceberg-ice shelf Fe source (Laufkötter et al., 2018; Person et al., 2019; Wadley et al., 2014).

Triggered by the melting and retreat of sea ice in spring and summer, the contribution of the sea-ice Fe reservoir to SO primary production is here relatively modest with increases of 5–6% over the seasonal ice zone in the CST, FLXCST, and FLXVAR experiments relative to CTL (Table 3). The FLXVAR2 experience almost doubles this contribution with a 10% increase. These lower estimates compared to those of Wadley et al. (2014) may be due to the absence of the Fe source from icebergs and ice shelves in our experiments. Indeed, a synergy between sea-ice formation and Fe delivered by ice shelves and icebergs may increase the Fe uptake by sea ice in fall and winter and its subsequent release for primary productivity.

Although nonlinear, but showing a clear trend in which higher primary productivity is associated with higher C export in the model (Person et al., 2019), the contribution of sea ice to primary productivity results in an increase in C export ranging from 9% to 19% in all four experiments relative to CTL. The increase in C export is at least twice as high as that of Wang et al. (2014), probably stemming from their significantly lower DFe uptake by sea ice in the SO. Our results suggest that the increase in particle export due to the fertilization effect of the sea-ice Fe source on phytoplankton photosynthesis may be largely non-negligible for air-sea CO<sub>2</sub> fluxes in the seasonal sea-ice-covered zone of the SO with important regional contributions as already highlighted (Tagliabue & Arrigo, 2005, 2016).

## 5. Conclusion

The impacts of three different formulations of DFe incorporation into sea ice on SO marine biogeochemistry were evaluated in a global ocean model. Large differences emerge in simulated Fe concentrations in sea ice. These however have little impact on the fertilization of surface waters by melting sea ice: The consistent representation of the mechanisms of Fe incorporation, transport and melting by sea ice, dominates the detailed distribution of Fe in sea ice. Current observations arguably favor the so-called FLXVAR formulation, in which ocean-ice Fe fluxes linearly increase with seawater Fe concentrations. In this formulation, sediments ultimately control Fe concentrations in sea ice, as well as the fertilization of the ocean by melting sea ice. Finally, the effect of Fe in sea ice of the SO on primary production varies from 5% to 10%, and the contribution to carbon export is from 9–19% among the different formulations. Such impacts suggest the need for future work, in particular the collection of new field observations.

## Data Availability Statement

Sea ice concentration data were retrieved from the Ocean and Sea Ice Satellite Application Facility center ([http://osisaf.met.no/p/ice/ice\\_conc\\_cdr\\_v2.html](http://osisaf.met.no/p/ice/ice_conc_cdr_v2.html)) and the corrected ocean color product from Australia's Integrated Marine Observing System (<http://imos.org.au/>). Model data are available at Zenodo (<https://doi.org/10.5281/zenodo.3824459>). Data of Fe in sea ice from Lannuzel et al. (2016) can be found online (at <https://doi.pangaea.de/10.1594/PANGAEA.865037>).

## Acknowledgments

This work is funded by the ANR project SOBUMS (ANR-16-CE01-0014) and was granted access to the HPC resources of IDRIS under the allocation 2019-A0060107451 made by GENCI. We thank two anonymous reviewers for their insightful and very detailed comments.

## References

- Ardyna, M., Claustre, H., Salle, J.-B., D'Ovidio, F., Gentili, B., van Dijken, G., et al. (2017). Delineating environmental control of phytoplankton biomass and phenology in the Southern Ocean. *Geophysical Research Letters*, *44*, 5016–5024. <https://doi.org/10.1002/2016GL072428>
- Ardyna, M., Lacour, L., Sergi, S., d'Ovidio, F., Sallée, J.-B., Rembauville, M., et al. (2019). Hydrothermal vents trigger massive phytoplankton blooms in the Southern Ocean. *Nature Communications*, *10*(1), 2451. <https://doi.org/10.1038/s41467-019-09973-6>
- Arrigo, K. R., Worthen, D. L., Lizotte, M. P., Dixon, P., & Dieckmann, G. (1997). Primary production in Antarctic sea ice. *Science*, *276*(5311), 394–397. <https://doi.org/10.1126/science.276.5311.394>
- Aumont, O., Ethé, C., Tagliabue, A., Bopp, L., & Gehlen, M. (2015). PISCES-v2: An ocean biogeochemical model for carbon and ecosystem studies. *Geoscientific Model Development*, *8*(8), 2465–2513. <https://doi.org/10.5194/gmd-8-2465-2015>
- Blain, S., Quéguiner, B., Armand, L., Belviso, S., Bombled, B., Bopp, L., et al. (2007). Effect of natural iron fertilization on carbon sequestration in the Southern Ocean. *Nature*, *446*(7139), 1070–1074. <https://doi.org/10.1038/nature05700>
- Blanke, B., & Delecluse, P. (1993). Variability of the tropical Atlantic Ocean simulated by a general circulation model with two different mixed-layer physics. *Journal of Physical Oceanography*, *23*(7), 1363–1388.
- Borrione, I., Aumont, O., Nielsdóttir, M. C., & Schlitzer, R. (2014). Sedimentary and atmospheric sources of iron around South Georgia, Southern Ocean: A modelling perspective. *Biogeosciences*, *11*, 1981–2001. <https://doi.org/10.5194/bg-11-1981-2014>
- Bouillon, S., Fichet, T., Legat, V., & Madec, G. (2013). The elastic-plastic method revisited. *Ocean Modelling*, *71*, 2–12. <https://doi.org/10.1016/j.ocemod.2013.05.013>
- Bowie, A. R., Maldonado, M. T., Frew, R. D., Croot, P. L., Achterberg, E. P., Mantoura, R. F. C., et al. (2001). The fate of added iron during a mesoscale fertilisation experiment in the Southern Ocean. *Deep Sea Research Part II: Topical Studies in Oceanography*, *48*(11), 2703–2743.
- Boyd, P. W. (2002). Environmental factors controlling phytoplankton processes in the Southern Ocean. *Journal of Phycology*, *38*(5), 844–861.
- Boyd, P. W., Arrigo, K. R., Strzpek, R., & van Dijken, G. L. (2012). Mapping phytoplankton iron utilization: Insights into Southern Ocean supply mechanisms. *Journal of Geophysical Research*, *117*, C06009. <https://doi.org/10.1029/2011JC007726>
- Boyd, P. W., & Ellwood, M. J. (2010). The biogeochemical cycle of iron in the ocean. *Nature Geoscience*, *3*(10), 675–682. <https://doi.org/10.1038/ngeo964>
- Boyd, P. W., Jickells, T., Law, C. S., Blain, S., Boyle, E. A., Buesseler, K. O., et al. (2007). Mesoscale iron enrichment experiments 1993–2005: Synthesis and future directions. *Science*, *315*(5812), 612–617. <https://doi.org/10.1126/science.1131669>
- Coale, K. H., Johnson, K. S., Chavez, F. P., Buesseler, K. O., Barber, R. T., Brzenski, M. A., et al. (2004). Southern Ocean iron enrichment experiment: Carbon cycling in high- and low-Si waters. *Science*, *304*(5669), 408–414. <https://doi.org/10.1126/science.1089778>
- Coon, M. D., Maykut, G. A., Pritchard, R. S., Rothrock, D. A., & Thorndike, A. S. (1974). Modeling the pack ice as an elastic-plastic material. *AIDJEX Bulletin*, *24*, 1–105.
- de Baar, H. J. W., de Jong, J. T. M., Bakker, D. C. E., Löscher, B. M., Veth, C., Bathmann, U., & Smetacek, V. (1995). Importance of iron for plankton blooms and carbon dioxide drawdown in the Southern Ocean. *Nature*, *373*(6513), 412–415. <https://doi.org/10.1038/373412a0>
- de Baar, H. J. W., de Jong, J. T. M., Nolting, R. F., Timmermans, K. R., van Leeuwe, M. A., Bathmann, U., et al. (1999). Low dissolved Fe and the absence of diatom blooms in remote Pacific waters of the Southern Ocean. *Marine Chemistry*, *66*(1), 1–34.
- de Boyer Montégut, C., Madec, G., Fischer, A. S., Lazar, A., & Iudicone, D. (2004). Mixed layer depth over the global ocean: An examination of profile data and a profile-based climatology. *Journal of Geophysical Research*, *109*, C12003. <https://doi.org/10.1029/2004JC002378>
- de Jong, J., Schoemann, V., Maricq, N., Mattielli, N., Langhorne, P., Haskell, T., & Tison, J.-L. (2013). Iron in land-fast sea ice of McMurdo Sound derived from sediment resuspension and wind-blown dust attributes to primary productivity in the Ross Sea, Antarctica. *Marine Chemistry*, *157*, 24–40. <https://doi.org/10.1016/j.marchem.2013.07.001>

- de Jong, J. T. M., Stammerjohn, S. E., Ackley, S. F., Tison, J.-L., Mattielli, N., & Schoemann, V. (2015). Sources and fluxes of dissolved iron in the Bellingshausen Sea (West Antarctica): The importance of sea ice, icebergs and the continental margin. *Marine Chemistry*, *177*, 518–535. <https://doi.org/10.1016/j.marchem.2015.08.004>
- Dethleff, D. (2005). Entrainment and export of Laptev Sea ice sediments, Siberian Arctic. *Journal of Geophysical Research*, *110*, C07009. <https://doi.org/10.1029/2004JC002740>
- Dinniman, M. S., St-Laurent, P., Arrigo, K. R., Hofmann, E. E., & Dijken, G. L. (2020). Analysis of iron sources in Antarctic continental shelf waters. *Journal of Geophysical Research: Oceans*, *125*, e2019JC015736. <https://doi.org/10.1029/2019JC015736>
- Duprat, L. P. A. M., Bigg, G. R., & Wilton, D. J. (2016). Enhanced Southern Ocean marine productivity due to fertilization by giant icebergs. *Nature Geoscience*, *9*(3), 219–221. <https://doi.org/10.1038/ngeo2633>
- Fraser, A. D., Massom, R. A., Michael, K. J., Galton-Fenzi, B. K., & Lieser, J. L. (2012). East Antarctic landfast sea ice distribution and variability, 2000–08. *Journal of Climate*, *25*(4), 1137–1156. <https://doi.org/10.1175/JCLI-D-10-05032.1>
- Fripiat, F., Meiners, K. M., Vancoppenolle, M., Papadimitriou, S., Thomas, D. N., Ackley, S. F., et al. (2017). Macro-nutrient concentrations in Antarctic pack ice: Overall patterns and overlooked processes. *Elementa: Science of the Anthropocene*, *5*(0), 13. <https://doi.org/10.1525/elementa.217>
- Garcia, H. E., Locarnini, R. A., Boyer, T. P., Antonov, J. I., Zweng, M. M., Baranova, O. K., & Johnson, D. R. (2010a). *World Ocean Atlas 2009 Volume 4: Nutrients (phosphate, nitrate, silicate)* Edited by Levitus, S. Washington, DC: NOAA Atlas NESDIS 71, U.S. Government Printing Office.
- Garcia, H. E., Locarnini, R. A., Boyer, T. P., Antonov, J. I., Zweng, M. M., Baranova, O. K., & Johnson, D. R. (2010b). *World Ocean Atlas 2009 Volume 3: Dissolved Oxygen, Apparent Oxygen Utilization, and Oxygen Saturation* Edited by Levitus, S. Washington, DC: NOAA Atlas NESDIS 70, U.S. Government Printing Office.
- Garrison, D. L., Close, A. R., & Reimnitz, E. (1989). Algae concentrated by frazil ice: Evidence from laboratory experiments and field measurements. *Antarctic Science*, *1*(4), 313–316. <https://doi.org/10.1017/S0954102089000477>
- Geibert, W., Assmy, P., Bakker, D. C. E., Hanfland, C., Hoppema, M., Pichevin, L. E., et al. (2010). High productivity in an ice melting hot spot at the eastern boundary of the Weddell Gyre. *Global Biogeochemical Cycles*, *24*, GB3007. <https://doi.org/10.1029/2009GB003657>
- Gent, P. R., & McWilliams, J. C. (1990). Isopycnal mixing in ocean circulation models. *Journal of Physical Oceanography*, *20*(1), 150–155.
- Gerringa, L. J. A., Alderkamp, A.-C., Laan, P., Thuróczy, C.-E., De Baar, H. J. W., Mills, M. M., et al. (2012). Iron from melting glaciers fuels the phytoplankton blooms in Amundsen Sea (Southern Ocean): Iron biogeochemistry. *Deep Sea Research Part II: Topical Studies in Oceanography*, *71*–76, 16–31. <https://doi.org/10.1016/j.dsr2.2012.03.007>
- Griffies, S. M., Biastoch, A., Böning, C., Bryan, F., Danabasoglu, G., Chassignet, E. P., et al. (2009). Coordinated Ocean-ice Reference Experiments (COREs). *Ocean Modelling*, *26*(1–2), 1–46. <https://doi.org/10.1016/j.ocemod.2008.08.007>
- Herraiz-Borreguero, L., Lannuzel, D., van der Merwe, P., Treverrow, A., & Pedro, J. B. (2016). Large flux of iron from the Amery Ice Shelf marine ice to Prydz Bay, East Antarctica. *Journal of Geophysical Research: Oceans*, *121*, 6009–6020. <https://doi.org/10.1002/2016JC011687>
- Hopwood, M. J., Carroll, D., Höfer, J., Achterberg, E. P., Meire, L., Le Moigne, F. A. C., et al. (2019). Highly variable iron content modulates iceberg-ocean fertilisation and potential carbon export. *Nature Communications*, *10*(1), 5261. <https://doi.org/10.1038/s41467-019-13231-0>
- Janssens, J., Meiners, K. M., Tison, J.-L., Dieckmann, G., Delille, B., & Lannuzel, D. (2016). Incorporation of iron and organic matter into young Antarctic sea ice during its initial growth stages. *Elementa: Science of the Anthropocene*, *4*, 000123. <https://doi.org/10.12952/journal.elementa.000123>
- Janssens, J., Meiners, K. M., Townsend, A. T., & Lannuzel, D. (2018). Organic matter controls of iron incorporation in growing sea ice. *Frontiers in Earth Science*, *6*, 22. <https://doi.org/10.3389/feart.2018.00022>
- Johnson, R., Strutton, P. G., Wright, S. W., McMinn, A., & Meiners, K. M. (2013). Three improved satellite chlorophyll algorithms for the Southern Ocean. *Journal of Geophysical Research: Oceans*, *118*, 3694–3703. <https://doi.org/10.1002/jgrc.20270>
- Key, R. M., Kozyr, A., Sabine, C. L., Lee, K., Wanninkhof, R., Bullister, J. L., et al. (2004). A global ocean carbon climatology: Results from Global Data Analysis Project (GLODAP). *Global Biogeochemical Cycles*, *18*, GB4031. <https://doi.org/10.1029/2004GB002247>
- Kovacs, A. (1996). Sea ice. Part 1. Bulk salinity versus ice floe thickness: U.S. Army Cold Regions Research and Engineering Lab, Hanover NH.
- Lancelot, C., Montety, A., Goosse, H., Becquevort, S., Schoemann, V., Pasquer, B., & Vancoppenolle, M. (2009). Spatial distribution of the iron supply to phytoplankton in the Southern Ocean: A model study. *Biogeosciences*, *6*, 2861–2878.
- Lannuzel, D., Bowie, A. R., van der Merwe, P. C., Townsend, A. T., & Schoemann, V. (2011). Distribution of dissolved and particulate metals in Antarctic sea ice. *Marine Chemistry*, *124*(1–4), 134–146. <https://doi.org/10.1016/j.marchem.2011.01.004>
- Lannuzel, D., Grotti, M., Abemoschi, M. L., & van der Merwe, P. (2015). Organic ligands control the concentrations of dissolved iron in Antarctic sea ice. *Marine Chemistry*, *174*, 120–130. <https://doi.org/10.1016/j.marchem.2015.05.005>
- Lannuzel, D., Schoemann, V., de Jong, J., Chou, L., Delille, B., Becquevort, S., & Tison, J.-L. (2008). Iron study during a time series in the western Weddell pack ice. *Marine Chemistry*, *108*(1–2), 85–95. <https://doi.org/10.1016/j.marchem.2007.10.006>
- Lannuzel, D., Schoemann, V., de Jong, J., Pasquer, B., van der Merwe, P., Masson, F., et al. (2010). Distribution of dissolved iron in Antarctic sea ice: Spatial, seasonal, and inter-annual variability. *Journal of Geophysical Research*, *115*, G03022. <https://doi.org/10.1029/2009JG001031>
- Lannuzel, D., Schoemann, V., de Jong, J., Tison, J.-L., & Chou, L. (2007). Distribution and biogeochemical behaviour of iron in the East Antarctic sea ice. *Marine Chemistry*, *106*(1–2), 18–32. <https://doi.org/10.1016/j.marchem.2006.06.010>
- Lannuzel, D., Vancoppenolle, M., van der Merwe, P., de Jong, J., Meiners, K. M., Grotti, M., et al. (2016). Iron in sea ice: Review and new insights. *Elementa: Science of the Anthropocene*, *4*, 000130. <https://doi.org/10.12952/journal.elementa.000130>
- Laufkötter, C., Stern, A. A., John, J. G., Stock, C. A., & Dunne, J. P. (2018). Glacial iron sources stimulate the Southern Ocean carbon cycle. *Geophysical Research Letters*, *45*, 13,377–13,385. <https://doi.org/10.1029/2018GL079797>
- Lavergne, T., Sørensen, A. M., Kern, S., Tonboe, R., Notz, D., Aaboe, S., et al. (2019). Version 2 of the EUMETSAT OSI SAF and ESA CCI sea-ice concentration climate data records. *The Cryosphere*, *13*(1), 49–78. <https://doi.org/10.5194/tc-13-49-2019>
- Lemieux, J.-F., Dupont, F., Blain, P., Roy, F., Smith, G. C., & Flato, G. M. (2016). Improving the simulation of landfast ice by combining tensile strength and a parameterization for grounded ridges. *Journal of Geophysical Research: Oceans*, *121*, 7354–7368. <https://doi.org/10.1002/2016JC012006>
- Lemieux, J.-F., Lei, J., Dupont, F., Roy, F., Losch, M., Lique, C., & Laliberté, F. (2018). The impact of tides on simulated landfast ice in a Pan-Arctic ice-ocean model. *Journal of Geophysical Research: Oceans*, *123*, 7747–7762. <https://doi.org/10.1029/2018JC014080>

- Lin, H., Rauschenberg, S., Hexel, C. R., Shaw, T. J., & Twining, B. S. (2011). Free-drifting icebergs as sources of iron to the Weddell Sea. *Deep Sea Research Part II: Topical Studies in Oceanography*, 58(11–12), 1392–1406. <https://doi.org/10.1016/j.dsr2.2010.11.020>
- Lipscomb, W. H. (2001). Remapping the thickness distribution in sea ice models. *Journal of Geophysical Research*, 106(C7), 13,989–14,000. <https://doi.org/10.1029/2000JC000518>
- Locarnini, R. A., Mishonov, A. V., Antonov, J. I., Boyer, T. P., Garcia, H. E., Baranova, O. K., et al. (2013). World Ocean Atlas 2013, Volume 1: Temperature. *NOAA Atlas NESDIS*, 73, 40.
- Madec, G. (2008). NEMO ocean engine. *Note du Pôle de modélisation de l'Institut Pierre-Simon Laplace, France*, 27, 1–217.
- Maksym, T. (2019). Arctic and Antarctic sea ice change: Contrasts, commonalities, and causes. *Annual Review of Marine Science*, 11(1), 187–213. <https://doi.org/10.1146/annurev-marine-010816-060610>
- Martin, J. H., Fitzwater, S. E., & Gordon, M. R. (1990). Iron deficiency limits phytoplankton growth in Antarctic waters. *Global Biogeochemical Cycles*, 4(1), 5–12.
- Martin, S., & Kauffman, P. (1981). A field and laboratory study of wave damping by grease ice. *Journal of Glaciology*, 27(96), 283–313.
- Moreau, S., Lannuzel, D., Janssens, J., Arroyo, M. C., Corkill, M., Cougnon, E., et al. (2019). Sea ice meltwater and circumpolar deep water drive contrasting productivity in three Antarctic polynyas. *Journal of Geophysical Research: Oceans*, 124, 2943–2968. <https://doi.org/10.1029/2019JC015071>
- Parkinson, C. L. (2019). A 40-y record reveals gradual Antarctic sea ice increases followed by decreases at rates far exceeding the rates seen in the Arctic. *Proceedings of the National Academy of Sciences*, 116(29), 14,414–14,423. <https://doi.org/10.1073/pnas.1906556116>
- Pellichero, V., Sallée, J.-B., Schmidtko, S., Roquet, F., & Charrassin, J.-B. (2017). The ocean mixed layer under Southern Ocean sea-ice: Seasonal cycle and forcing. *Journal of Geophysical Research: Oceans*, 122, 1608–1633. <https://doi.org/10.1002/2016JC011970>
- Person, R., Aumont, O., & Lévy, M. (2018). The biological pump and seasonal variability of pCO<sub>2</sub> in the Southern Ocean: Exploring the role of diatom adaptation to low iron. *Journal of Geophysical Research: Oceans*, 123, 3204–3226. <https://doi.org/10.1029/2018JC013775>
- Person, R., Aumont, O., Madec, G., Vancoppenolle, M., Bopp, L., & Merino, N. (2019). Sensitivity of ocean biogeochemistry to the iron supply from the Antarctic Ice Sheet explored with a biogeochemical model. *Biogeosciences*, 16, 3583–3603. <https://doi.org/10.5194/bg-16-3583-2019>
- Pörtner, H. O., Roberts, D. C., Masson-Delmotte, V., Zhai, P., Tignor, M., Poloczanska, E., et al. (2019). IPCC special report on the ocean and cryosphere in a changing climate: IPCC.
- Prather, M. J. (1986). Numerical advection by conservation of second-order moments. *Journal of Geophysical Research*, 91(D6), 6671–6681. <https://doi.org/10.1029/JD091iD06p06671>
- Raiswell, R., Hawkings, J. R., Benning, L. G., Baker, A. R., Death, R., Albani, S., et al. (2016). Potentially bioavailable iron delivery by iceberg-hosted sediments and atmospheric dust to the polar oceans. *Biogeosciences*, 13, 3887–3900. <https://doi.org/10.5194/bg-13-3887-2016>
- Raiswell, R., Hawkings, J., Elsenousy, A., Death, R., Tranter, M., & Wadham, J. (2018). Iron in glacial systems: Speciation, reactivity, freezing behavior, and alteration during transport. *Frontiers in Earth Science*, 6(222). <https://doi.org/10.3389/feart.2018.00222>
- Rintoul, S. R., Chown, S. L., DeConto, R. M., England, M. H., Fricker, H. A., Masson-Delmotte, V., et al. (2018). Choosing the future of Antarctica. *Nature*, 558(7709), 233–241. <https://doi.org/10.1038/s41586-018-0173-4>
- Rousset, C., Vancoppenolle, M., Madec, G., Fichefet, T., Flavoni, S., Barthélemy, A., et al. (2015). The Louvain-La-Neuve sea ice model LIM3.6: Global and regional capabilities. *Geoscientific Model Development*, 16. <https://doi.org/10.5194/gmd-8-2991-2015>
- Sallée, J.-B., Shuckburgh, E., Bruneau, N., Meijers, A. J. S., Bracegirdle, T. J., & Wang, Z. (2013). Assessment of Southern Ocean mixed-layer depths in CMIP5 models: Historical bias and forcing response. *Journal of Geophysical Research: Oceans*, 118, 1845–1862. <https://doi.org/10.1002/jgrc.20157>
- Schlitzer, R., Anderson, R. F., Dodas, E. M., Lohan, M., Geibert, W., Tagliabue, A., et al. (2018). The GEOTRACES intermediate data product 2017. *Chemical Geology*, 493, 210–223. <https://doi.org/10.1016/j.chemgeo.2018.05.040>
- Sedwick, P. N., & DiTullio, G. R. (1997). Regulation of algal blooms in Antarctic Shelf Waters by the release of iron from melting sea ice. *Geophysical Research Letters*, 24(20), 2515–2518. <https://doi.org/10.1029/97GL02596>
- Smetacek, V. (2001). EisenEx: International team conducts iron experiment in Southern Ocean. *U.S. JGOFS Newsletter*, 11(1), 11–14.
- Tagliabue, A., & Arrigo, K. R. (2005). Iron in the Ross Sea: 1. Impact on CO<sub>2</sub> fluxes via variation in phytoplankton functional group and non-Redfield stoichiometry. *Journal of Geophysical Research*, 110, C03009. <https://doi.org/10.1029/2004JC002531>
- Tagliabue, A., Bopp, L., & Aumont, O. (2009). Evaluating the importance of atmospheric and sedimentary iron sources to Southern Ocean biogeochemistry. *Geophysical Research Letters*, 36, L13601. <https://doi.org/10.1029/2009GL038914>
- Tagliabue, A., Bowie, A. R., Boyd, P. W., Buck, K. N., Johnson, K. S., & Saito, M. A. (2017). The integral role of iron in ocean biogeochemistry. *Nature*, 543(7643), 51–59. <https://doi.org/10.1038/nature21058>
- Tagliabue, A., & Kevin, R. (2016). Decadal trends in air-sea CO<sub>2</sub> exchange in the Ross Sea (Antarctica). *Geophysical Research Letters*, 43, 5271–5278. <https://doi.org/10.1002/2016GL069071>
- Tagliabue, A., Mtshali, T., Aumont, O., Bowie, A. R., Klunder, M. B., Roychoudhury, A. N., & Swart, S. (2012). A global compilation of dissolved iron measurements: Focus on distributions and processes in the Southern Ocean. *Biogeosciences*, 9, 2333–2349. <https://doi.org/10.5194/bg-9-2333-2012>
- Thorndike, A. S., Rothrock, D. A., Maykut, G. A., & Colony, R. (1975). The thickness distribution of sea ice. *Journal of Geophysical Research*, 80(33), 4501–4513. <https://doi.org/10.1029/JC080i033p04501>
- van der Merwe, P., Lannuzel, D., Bowie, A. R., & Meiners, K. M. (2011). High temporal resolution observations of spring fast ice melt and seawater iron enrichment in East Antarctica. *Journal of Geophysical Research*, 116, G03017. <https://doi.org/10.1029/2010JG001628>
- Vancoppenolle, M., Fichefet, T., Goosse, H., Bouillon, S., Madec, G., & Maqueda, M. A. M. (2009). Simulating the mass balance and salinity of Arctic and Antarctic sea ice. 1. Model description and validation. *Ocean Modelling*, 27(1–2), 33–53. <https://doi.org/10.1016/j.ocemod.2008.10.005>
- Vancoppenolle, M., Goosse, H., de Montety, A., Fichefet, T., Tremblay, B., & Tison, J.-L. (2010). Modeling brine and nutrient dynamics in Antarctic sea ice: The case of dissolved silica. *Journal of Geophysical Research*, 115, C02005. <https://doi.org/10.1029/2009JC005369>
- Vancoppenolle, M., Meiners, K. M., Michel, C., Bopp, L., Brabant, F., Carnat, G., et al. (2013). Role of sea ice in global biogeochemical cycles: emerging views and challenges. *Quaternary Science Reviews*, 79, 207–230. <https://doi.org/10.1016/j.quascirev.2013.04.011>
- Wadley, M. R., Jickells, T. D., & Heywood, K. J. (2014). The role of iron sources and transport for Southern Ocean productivity. *Deep Sea Research Part I: Oceanographic Research Papers*, 87, 82–94. <https://doi.org/10.1016/j.dsr.2014.02.003>
- Wagener, T., Guieu, C., Losno, R., Bonnet, S., & Mahowald, N. (2008). Revisiting atmospheric dust export to the Southern Hemisphere ocean: Biogeochemical implications. *Global Biogeochemical Cycles*, 22, GB2006. <https://doi.org/10.1029/2007GB002984>

- Wang, S., Bailey, D., Lindsay, K., Moore, J. K., & Holland, M. (2014). Impact of sea ice on the marine iron cycle and phytoplankton productivity. *Biogeosciences*, *11*, 4713–4731. <https://doi.org/10.5194/bg-11-4713-2014>
- Worby, A. P., Geiger, C. A., Paget, M. J., Woert, M. L. V., Ackley, S. F., & DeLiberty, T. L. (2008). Thickness distribution of Antarctic sea ice. *Journal of Geophysical Research*, *113*, C05S92. <https://doi.org/10.1029/2007JC004254>
- Zweng, M. M., Reagan, J. R., Antonov, J. I., Locarnini, R. A., Mishonov, A. V., Boyer, T. P., et al. (2013). World Ocean Atlas 2013, Volume 2: Salinity. *NOAA Atlas NESDIS*, *74*, 39.